

เซรามิกฟรี-สเตอร์สที่มีโครงสร้างผสมระหว่างมัลไลต์และอะลูมินา



นางสาว วีนัสรินทร์ อินทร์ดียะ

สถาบันวิทยบริการ
จุฬาลงกรณ์มหาวิทยาลัย

วิทยานิพนธ์นี้เป็นส่วนหนึ่งของการศึกษาตามหลักสูตรปริญญาวิทยาศาสตรมหาบัณฑิต

สาขาวิชา เทคโนโลยีเซรามิก ภาควิชาวัสดุศาสตร์

คณะวิทยาศาสตร์ จุฬาลงกรณ์มหาวิทยาลัย

ปีการศึกษา 2547

ISBN 974-17-6387-5

ลิขสิทธิ์ของจุฬาลงกรณ์มหาวิทยาลัย

PRE-STRESSED CERAMICS WITH HYBRID STRUCTURE OF MULLITE AND ALUMINA



Miss Weenusarin Intiya

สถาบันวิทยบริการ
จุฬาลงกรณ์มหาวิทยาลัย

A Thesis Submitted in Partial Fulfillment of the Requirements
for the Degree of Master of Science Program in Ceramic Technology

Faculty of Science

Chulalongkorn University

Academic Year 2004

ISBN 974-17-6387-5

Thesis Title Pre-stressed ceramics with hybrid structure of mullite and alumina
By Miss Weenusarin Intiya
Filed of study Ceramic Technology
Thesis Advisor Professor Shigetaka Wada, Ph. D.
Thesis Co-advisor Associate Professor Supatra Jinawath, Ph. D.

Accepted by the Faculty of Science, Chulalongkorn University in Partial Fulfillment of the Requirements for the Master's Degree

..... Dean of the Faculty of science
(Professor Piamsak Menasveta, PH.D.)

THESIS COMMITTEE

..... Chairman
(Associate Professor Saowaroj Chuayjuljit)

..... Thesis Advisor
(Professor Shigetaka Wada, Ph. D.)

..... Thesis Co-advisor
(Associate Professor Supatra Jinawath, Ph. D.)

..... Member
(Sirithan Jiemsirilers, Ph. D.)

..... Member
(Dujreutai Pongkao, Ph. D.)

วินัสรินทร์ อินทร์ดิยะ : เซรามิกพรี-สเตรสที่มีโครงสร้างผสมระหว่างมัลไลต์และอะลูมินา

(PRE-STRESSED CERAMICS WITH HYBRID STRUCTURE OF MULLITE AND ALUMINA)

อ. ที่ปรึกษา: ศ.ดร. ชีเกดากะ วาดะ, อ.ที่ปรึกษาร่วม : รศ.ดร. สุพัตรา จินาวัฒน์ จำนวน 63 หน้า.

ISBN 974-17-6387-5.

วัสดุเซรามิกเป็นวัสดุที่มีความเปราะ เนื่องจากพันธะทางเคมีส่วนใหญ่เป็นพันธะไอออนิกและโควาเลนต์ จึงทำให้มีข้อจำกัดในการนำไปใช้งาน ดังนั้นการปรับปรุงและพัฒนาวัสดุเซรามิกให้มี toughness และความแข็งแรงเพิ่มขึ้นจึงเป็นการลดข้อจำกัดดังกล่าว ทำให้วัสดุเซรามิกสามารถนำไปใช้งานได้กว้างขวางและหลากหลายมากขึ้น

ปัจจุบันการเพิ่มคุณสมบัติเชิงกลให้กับวัสดุเซรามิกมีหลายวิธีด้วยกัน และในงานวิจัยนี้ได้ศึกษาถึงกระบวนการปรับปรุงสมบัติทางกลของวัสดุโดยขึ้นรูปเป็นวัสดุเชิงประกอบที่มีหลายชั้น และได้เลือกใช้การขึ้นรูปด้วยวิธีการอัดและการหล่อ ใช้ผงอะลูมินา A-21 และผงมัลไลต์ KM102 เป็นวัตถุดิบเริ่มต้น จากนั้นทำการบดเพื่อลดขนาดด้วยเอทริชันมิลล์ และนำผงที่ได้หลังทำการบดมาผสมในบอลมิลล์ในอัตราส่วน A-21/ KM102 เท่ากับ 0/100 ถึง 100/0 เปรอร์เซ็นต์โดยน้ำหนัก หลังการขึ้นรูปทำการเผาซินเทอร์ในช่วง 1650-1700 องศาเซลเซียส เป็นเวลา 2 ชั่วโมง

วัสดุเชิงประกอบที่ขึ้นรูปโดยการอัดเกือบทุกชิ้นตัวอย่างเกิดการแตกหักหลังเผาซินเทอร์ และเมื่อขึ้นรูปโดยการหล่อเกิดการแตกหักหลังซินเทอร์เช่นกัน เนื่องจากผลของความเค้นตกค้างที่เกิดจากผลต่างของค่าสัมประสิทธิ์การขยายตัวเนื่องจากความร้อนระหว่างอะลูมินาและมัลไลต์ จากผลดังกล่าว การทำเป็นวัสดุเชิงประกอบที่มีหลายชั้นและมีโครงสร้างแบบผสม จึงไม่สามารถเพิ่มสมบัติความแข็งแรงให้กับวัสดุเซรามิก

อย่างไรก็ตามวัสดุเชิงประกอบที่มีอัตราส่วนผสม A-21/KM102 เท่ากับ 40/60 เปรอร์เซ็นต์โดยน้ำหนักแสดงสมบัติที่สำคัญคือ 1) ให้โครงสร้างทางจุลภาคที่มีความสม่ำเสมอ 2) ให้ค่า toughness ที่สูงถึง $4.4 \text{ MPa}\cdot\text{m}^{1/2}$ 3) ให้ค่าความแข็งแรงดัด 282 เมกะปาสกาล

ภาควิชาวัสดุศาสตร์

สาขาวิชา เทคโนโลยีเซรามิก

ปีการศึกษา 2547

ลายมือชื่อนิสิต.....

ลายมือชื่ออาจารย์ที่ปรึกษา.....

ลายมือชื่ออาจารย์ที่ปรึกษาร่วม.....

4572500923 : MAJOR CERAMIC TECHNOLOGY

KEY WORD : ALUMINA-MULLITE COMPOSITE/ PRE-STRESSED CERAMICS/ MULTI-LAYER/ MECHANICAL STRENGTH

WEENUSSARIN INTIYA: PRE-STRESSED CERAMICS WITH HYBRID STRUCTURE OF MULLITE AND ALUMINA, THESIS ADVISOR: PROF. SHIGETAKA WADA, Ph.D., THESIS COADVISOR : ASSOC. PROF. SUPATRA JINAWATH, Ph.D., 63 pp. ISBN 974-17-6387-5.

Most ceramic materials are inherently low fracture toughness and show extremely limited plastic deformation, because their chemical bondings are ionic and covalent. Hence, improvements of toughness as well as the strength of ceramic materials are necessary for a broader range of application.

In this research, we concentrated on increasing strength and toughness of ceramic materials by multilayer-ceramic composite method. Die-pressing and slip casting were our selected processes. Alumina and mullite were selected as the starting materials and the attrition mill was used to reduce the particle size of these powders. The compositions of A-21/KM102 specimens were varied from 0/100 to 100/0 wt%. They were prepared by ball mill mixing and sintered at temperature ranging from 1650-1700 °C for 2 hours.

The die pressed multi-layered specimens were almost broken after sintering. The slip cast multi-layered tube specimens were also broken by the residual stress caused by the difference of thermal expansions. As a result, we concluded that this kind of hybrid structure is not a good solution to get high strength ceramics.

On the other hand, the composite with 40A/60M wt% ratio showed (1) a homogeneous microstructure (without abnormal grain growth), (2) a rather higher K_{IC} of 4.4 MPa.m^{1/2} and (3) a good bending strength of 282 MPa.

Department Materials

Field of study Ceramic Technology

Academic year 2004

ScienceStudent's

Advisor's signature.....

Co-advisor's signature.....

ACKNOWLEDGEMENTS

I would like to express my sincere gratitude to my advisor, Professor Dr. Shigetaka Wada, for his encouragement, suggestion and for all that I have learnt from him throughout this research. His advice inspired the good idea and motivated the research to be completed. I would like to extend my gratitude to my co-advisor, Associated Professor Dr. Supatra Jinawath, who gave me a good advice and my research would not be completed without her invaluable suggestions.

I would like to thank my thesis committees, for their time to review this thesis and their valuable comments. Furthermore, my thanks are also extended to my friends at the Department of Material Science, especially Mr. Apirat Theerapapvisetpong, Miss Luksana Kreethawate, Miss Kannika Hatthapanit, Miss Piyaporn Chaiyapuck, Miss Usa Kaeowwanpen, Mr. Nirut Wungmooklang and Miss Khantima Hemra, for their friendship and supports.

Finally, I would like to express my most sincere gratitude to my parents, for their unconditional love, encouragement and understanding.

สถาบันวิทยบริการ
จุฬาลงกรณ์มหาวิทยาลัย

CONTENTS

| | Page |
|--|-----------|
| Abstract (Thai)..... | iv |
| Abstract (English)..... | v |
| Acknowledgements..... | vi |
| Contents..... | vii |
| List of tables..... | x |
| List of figures..... | xi |
| Chapter1 Introduction..... | 1 |
| 1.1 Introduction..... | 1 |
| 1.2 Objective..... | 2 |
| Chapter 2 Literature reviews..... | 3 |
| 2.1 Compression glaze | 3 |
| 2.2 Tempering of glass by air blowing..... | 4 |
| 2.3 Ion – exchange scuffing process..... | 6 |
| 2.4 Layered ceramics with different thermal expansion..... | 8 |
| 2.5 Functionally graded materials (FGM _s)..... | 9 |
| Chapter 3 Experimental Procedure..... | 10 |
| 3.1 Experimental flowchart | 10 |
| 3.2 Raw materials and characterization..... | 13 |
| 3.2.1 Raw materials..... | 13 |
| 3.2.2 Raw materials characterization..... | 15 |
| 3.2.2.1 Particle size distribution determination..... | 15 |
| 3.2.2.2 Specific surface area measurement..... | 15 |
| 3.2.2.3 X-Ray diffraction analysis..... | 15 |
| 3.3 Composition and preparation of Alumina-mullite composite powder..... | 15 |

CONTENTS (cont.)

| | Page |
|---|------------|
| 3.4 Slip cast conditions of Alumina-mullite 2-layered tube and plate..... | comp 16 |
| 3.5 Characterization of sintered specimens..... | 17 |
| 3.5.1 Shrinkage..... | 17 |
| 3.5.2 Bulk density, water absorption and relative density..... | 18 |
| 3.5.3 Microstructure examination by SEM..... | 19 |
| 3.5.4 Vickers hardness and fracture toughness | 20 |
| 3.5.5 Strength and Young's modulus | 20 |
| Chapter 4 Experimental result and discussion..... | 22 |
| 4.1 Raw materials characterization..... | 22 |
| 4.1.1 Particle size distribution determination..... | 22 |
| 4.1.2 Specific surface area measurement | 25 |
| 4.1.3 X-Ray diffraction analysis..... | 25 |
| 4.2 Preliminary sintering of Alumina and mullite | 28 |
| 4.3 Sintering a 2-layer pellet formed by die pressing..... | 30 |
| 4.4 Sintering a 2-layer tube formed by slip casting..... | 32 |
| 4.5 Characterization of sintered ceramics..... | 34 |
| 4.5.1 Shrinkage..... | 34 |
| 4.5.2 Bulk density, water absorption and relative density..... | 35 |
| 4.5.3 Microstructure of sintered specimen by SEM..... | 36 |
| 4.5.4 Thermal Expansion coefficient of the specimens..... | 39 |
| 4.5.5 Young's modulus..... | 41 |
| 4.5.6 Vickers hardness and fracture toughness..... | 42 |
| 4.5.7 Bending strength..... | 45 |

CONTENTS (cont.)

| | Page |
|----------------------------|------|
| Chapter 5 Conclusion..... | 50 |
| Chapter 6 Future work..... | 51 |
| References..... | 52 |
| Appendices..... | 54 |
| Appendix A..... | 55 |
| Appendix B..... | 58 |
| Biography..... | 63 |



สถาบันวิทยบริการ
จุฬาลงกรณ์มหาวิทยาลัย

LIST OF TABLES

| | Page |
|--|------|
| Table 3.1 Typical properties of alumina A-21..... | 14 |
| Table 3.2 Typical properties of mullite KM102 and 70M..... | 14 |
| Table 3.3 Compositions of the Alumina-mullite composite..... | 15 |
| Table 3.4 Compositions of alumina and mullite slurries to fabricated 2-layer tube Composite | 17 |
| Table 3.5 Theoretical density of each composite from calculation Table 4.1 Specific surface area of powder as starting materials..... | 18 |
| Table 4.1 Specific surface area of powders..... | 25 |
| Table 4.2 Show the pictures of 2- layer pellet specimens, formed by die pressing and sintered at 1650 C 2 h..... | 31 |
| Table 4.3 the picture of 3-layer pellet specimen formed by die-pressing and sintered at 1650 C 2 h..... | 32 |
| Table 4.4 picture of 2-layer tube specimens (Process 1) formed by slip casting and sintered at 1650 C for 2h..... | 33 |
| Table 4.5 picture of 2-layer tube specimens (Process 2), formed by slip casting and sintered at 1650 C for 2h..... | 33 |
| Table 4.6 Volume shrinkage and Linear shrinkage of specimens sintered at 1650 C 2h..... | 34 |

LIST OF FIGURES

| | Page |
|--|------|
| Fig.2.1 Distribution of internal stress in glazed plates..... | 4 |
| Fig.2.2 Stress distribution in tempered glass plates..... | 5 |
| Fig 2.3 Stress distribution in the wall of a glass object strengthened by ion-exchange..... | 7 |
| Fig 3.1(a) Experimental flowchart of starting powder preparation and selection..... | 10 |
| Fig 3.1(b) Experimental flowchart, step2, 2-layered pellet composites preparation..... | 11 |
| Fig 3.1(c) Experimental flowchart, step3, slip casting preparation..... | 12 |
| Fig 3.1(d) Experimental flowchart, step4 characterization..... | 13 |
| Fig 3.2 Flow chart of sample preparation for SEM observation..... | 19 |
| Fig 3.3 schematically of 4- point bending test..... | 20 |
| Fig 4.1 Particle size distribution of mullite 70M (a) and mullite KM102 (b) sampling at various periods of milling time..... | 23 |
| Fig 4.2 Particle size distribution of mullite 70M (a) and mullite KM102(b) milled 10h with alumina balls..... | 24 |
| Fig. 4.3 X-Ray diffraction patterns of raw mullite (a)70M, (b)70M milled 10 h, (c) raw mullite KM102 and (d) KM102 milled 10 h..... | 27 |
| Fig. 4.4 The relationship between (a) bulk density and (b) relative density with temperature for various starting materials..... | 29 |
| Fig. 4.5 volume shrinkage of starting materials at various temperatures..... | 29 |
| Fig 4.6 Bulk density (a) and relative density (b) of specimens formed by slip casting, sintered at 1650 and 1700 °C for 2h. at a heating rate of 5°C/min..... | 35 |
| Fig 4.7 water absorption of specimens formed by slip casting, sintered at 1650 and 1700 °C for 2h. at a heating rate of 5°C/min..... | 36 |
| Fig. 4.8 SEM micrographs of sintered slip cast specimens at 1700 °C, 2 h, (a) A-21, (b) KM102 and (c) composite of 40 wt% of alumina..... | 37 |
| Fig 4.9 Grain sizes of specimens sintered at 1650 and 1700 °c, 2h..... | 38 |
| Fig. 4.10 show the average of Thermal Expansion Coefficient (TEC) 25-1000 C (a) the TEC at various temperatures (b) the comparison of TEC values between the experimental and reference..... | 40 |

LIST OF FIGURES (Cont.)

| | Page |
|--|------|
| Fig. 4.11 Young's modulus of specimens formed by die pressing and slip casting, sintered at 1650 and 1700°C for 2h..... | 41 |
| Fig. 4.12 Vicker's hardness of specimens formed by die pressing and slip casting..... | 42 |
| Fig. 4.13 Fracture toughness of specimens formed by die pressing or slip casting..... | 43 |
| Fig. 4.14. SEM micrographs of 60 wt% of Al ₂ O ₃ specimen sintered at 1700°C for 2h, (a) formed by die pressing and (b) formed by slip casting process..... | 44 |
| Fig. 4.15 Bending strength of specimens formed by slip casting, sintered at 1650 and 1700°C for 2h..... | 46 |
| Fig. 4.16 Bending strength of specimens formed by die pressing, sintered at 1650 and 1700°C for 2h..... | 46 |
| Fig. 4.17. SEM micrographs of composite specimens formed by die pressing process, sintered at 1650 °C and 1700 °C for 2 h. | 47 |
| Fig. 4.18 comparison of the bending strength between only polished (P) and polished followed by annealing (P+A) of specimens formed by die pressing, were sintered at 1650°C for 2h..... | 48 |
| Fig. 4.19 comparison the bending strength between only polished (P) and annealed followed by polishing (A+P) of specimens formed by slip casting, were sintered at 1650°C for 2h..... | 48 |

CHAPTER 1

INTRODUCTION

1.1 Introduction

Most ceramic materials are inherently low in fracture toughness and show extremely limited plastic deformation, because their chemical bondings are ionic and covalent. Hence, improvements of toughness as well as the strength of ceramic materials are necessary for wide application [1].

There are many special processes or techniques to improve the mechanical properties of ceramic materials. They are divided into the following groups: 1) Reducing the size of critical flaws. 2) Increasing the resistance to crack propagation. 3) Creation of protective surface layers. 4) Suppressing unfavorable inner stresses or creating a suitable compressive prestress [2].

In this research, we concentrate on the increasing strength and toughness of ceramic materials by multi-layered ceramic composite method. When ceramics with different coefficients of thermal expansion (CTE) are formed into a multi-layered ceramic and sintered at high temperature, the layer with lower CTE is in the compression state after cooling to room temperature, inversely the layer with higher CTE is in the tension state. This mechanism is similar to high tension porcelain with compression glaze, tempered glass with high compressive strength and chemically tempered glass [2]. Die pressing and slip casting are selected fabrication processes in this research. Alumina and mullite are selected as the starting materials, because they have different coefficients of thermal expansion.

Alumina (Al_2O_3) is one of the very popular structural ceramic materials that is widely used in the field of structural applications. The superior mechanical properties such as high strength, high hardness, high electrical resistance, good chemical durability, good corrosion resistance and good wear resistance make alumina an important role in the

structural work such as media ball, substrate for integrated circuit, cutting tool, crucibles etc. The coefficients of thermal expansion is $8.8 \times 10^{-6} \text{ }^{\circ}\text{C}^{-1}$ [3].

Mullite ($3\text{Al}_2\text{O}_3 \cdot 2\text{SiO}_2$) is an aluminosilicate ceramic material which is a good candidate material for a high temperature structural application, because of its excellent physical properties, such as, high temperature mechanical stability, high creep resistance and high thermal shock resistance [4,5]. In addition, nowadays mullite can be synthesized in Thailand by using silica from rice husk and alumina. So, in the future we can get inexpensive mullite powder for using in the research of mullite materials too. The coefficients of thermal expansion is $5.3 \times 10^{-6} \text{ }^{\circ}\text{C}^{-1}$ [3].

From the above mentioned, it is expected that composite materials with multi-layered structure having high mechanical strength will be fabricated in this research.

1.2 The objectives of this research are;

- 1) To know the effect of the coefficients of thermal expansion mismatch on the mechanical properties of multi-layered ceramics.
- 2) To develop technology making the multi-layered ceramics without cracking.
- 3) To characterize the basic properties of alumina-mullite composite.

CHAPTER 2

LITERATURE REVIEWS

Glass and ceramics are reinforced microscopically and macroscopically. In this chapter, the mechanism and technology of macroscopic reinforcement and toughening are reviewed.

2.1 Compression glaze

The increasing of strength and the resistance to damage or failure of ceramic components are realized by several techniques. The creation of protective surface layer is one of the method to improve the mechanical property of ceramics, that is not to increase the strength itself but to reduce the stresses in the surface layer or to mitigate the damage of the surface which represents in the most sensitive parts of ceramics.

Protective surface layers are usually formed at high temperatures and often have coefficients of thermal expansion different from that of the bulk. Stresses are generated in them during cooling and these remain locked in the article permanently. For example, the strengthening glazes, this stress is intentionally created, but often it is really just an accompanying effect. So, it is important to know at least its approximate magnitude in order to be able to predict the behavior and to optimize some parameters. Such as, composition, thickness and the method of preparation of the protective layer.

From Fig.2.1 Shown in the next page, the stresses acting in the glaze and in the body at points distant from the ends may be described by equation (2.1)

$$\sigma_g = \frac{(\alpha_g - \alpha_s)\Delta T}{\frac{1 - \nu_g}{E_g} + \frac{1 - \nu_s}{E_s} \left(\frac{h_g}{h_s}\right)} \quad \sigma_s = -\sigma_g \left(\frac{h_g}{h_s}\right) \dots\dots\dots (2.1)$$

Where: subscript **g** indicates the glaze, subscript **s** indicates the body.

σ = The stress

h = Thickness

α = The coefficients of thermal expansion

E = Young's modulus

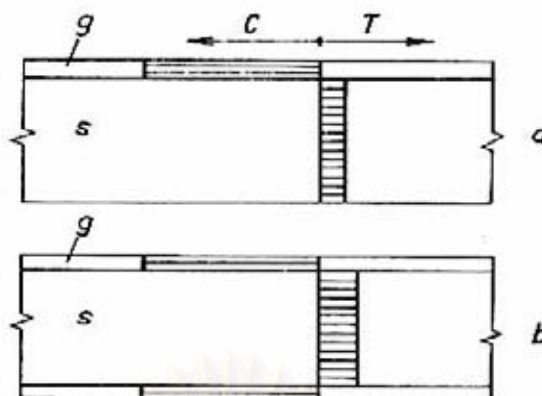


Fig. 2.1. Distribution of internal stress in glazed plates. a=one-side glazed plate, b=two-side glazed plate, s=substrate, g=glaze, T=tension, C=compression.

From equation (2.1) the stress in the coating will be compressive ($\sigma_g < 0$), when the coefficients of thermal expansion of the coating is lower than that of the substrate ($\alpha_g < \alpha_s$). Further, this stress becomes higher with larger $\Delta\alpha = (\alpha_g - \alpha_s)$, ΔT , h_g/h_s and higher Young's modulus.

In this study we have considered only stresses generated by the difference between the coefficients of thermal expansion of the coating and bulk. However, if the body is also loaded by external forces or is exposed to temperature change, further stresses arise in it. The resultant stress in the coating or in the body is given by equation (2.2)

$$\sigma(x) = \sigma_{int}(x) + \sigma_{ext}(x) \quad \dots\dots\dots (2.2)$$

Where $\sigma_{int}(x)$ = The internal stress, calculated according to equation (2.1)

$\sigma_{ext}(x)$ = The external stress by load

2.2 Tempering of glass by air blowing

This kind of strengthening mechanism occurs when the glass article is heated up to a temperature near the softening point and then rapidly cooled by air jet or immersed in a liquid medium for instance, molten tin, molten salts or oils. On cooling the hot glass, a temperature gradient is formed between the cooler surface and warmer interior. At this time,

the inner warmer layers of the glass continue to contract. This contraction, however, is opposed by the cold surface layers which give rise to a system of stresses, compressive at the surface and tensile in the interior. Since the glass is already rigid, these stresses cannot be equalized and remain locked in the glass permanently [2, 3].

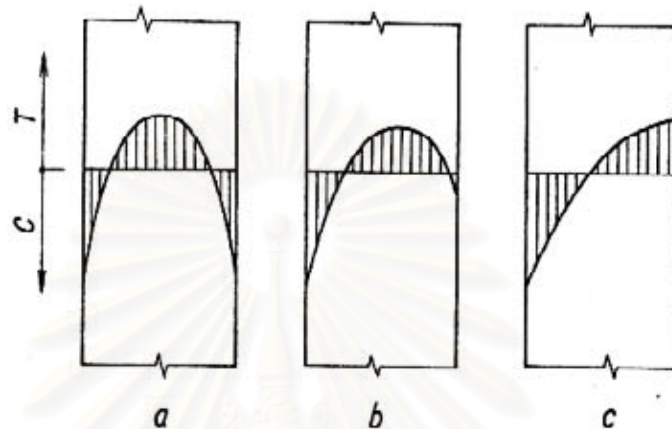


Fig. 2.2. Stress distribution in tempered glass plates, a=the cooling was symmetrical at both sides, b,c=the left surface was cooled more intensively, t=tension ,c=compression

The glass plate is cooled symmetrically from both surface, if the cooling intensity is not too high, the stress within the plate has parabolic distribution according to

Fig.2.2 (a).

$$\sigma(x) = \frac{\alpha E}{1-\nu} T_g \cdot K \left(1 - 12 \frac{x^2}{h^2}\right) \dots\dots\dots (2.3)$$

Where: T_g = The transformation temperature of the glass

x = The distance from the middle plane

K = a parameter characterizing the cooling rate.

From equation (2.3) the stress increases with growing elastic modulus (E), the coefficients of thermal expansion (α), and the thickness of glass (h). The effect of glass thickness is rather strong. According to equation (2.3), increasing the wall thickness by a factor of two without any change in the cooling conditions causes the compressive stress to quadruple.

The strength of tempered glass is given approximately by equation (2.4)

$$\sigma = \sigma_0 + \sigma_c \quad \dots\dots\dots (2.4)$$

Where: σ_0 = The initial strength of the unstrengthened body

σ_c = The compressive surface stress

The strength achieved by tempering depends on the shape and size of the article, the glass type and the means of cooling. Flat glass of common thickness and air cooling yields bending strength up to 300-400 MPa and in the common production about 200-250 MPa [2, 20]. The strengthening degree is lower with articles of complex shape since it is very difficult to attain an appropriate stress distribution in all parts of the body. For higher strength requirements, another kind of strengthening may be more appropriate, for example ion-exchange stuffing process, surface crystallization process etc.

2.3 Ion-exchange stuffing process

Glasses and crystalline ceramics can be strengthened by developing a state of compression in the surface regions of the materials. Surface ion-exchange process, which is also called chemical strengthening method, consists in the exposure of the article for a certain time to the action of an agent that having an appropriate composition and temperature. In this way, the surface layer of the glass changes gradually its chemical composition and properties.

There are two groups of chemical strengthening methods according to whether the ion-exchange is realized at temperatures higher or lower than the strain point.

2.3.1 Ion-exchange above the strain point

The alkali metal ions (Na^+ , K^+) in the surface layer of the glass are replaced by other monovalent ions so that a glass with a lower thermal expansion than the bulk glass is created here. In the exchange of ions with a different diameter leads to stress generation in the glass. But at the high temperature used, this stress is rapidly released, so that the glass

remains without stress during the process. After the glass has cooled down, owing to its lower expansion, causes the contraction during the cooling less than the original bulk glass, so a compressive stress acts in the surface layer.

Owing to a number of disadvantages (expensive lithium salts, or small degree of strengthening and only thin compressive layer in other cases), this kind of strengthening is used rarely, or only in combination with other methods.

2.3.2 Ion-exchange below the strain point

The alkali ions in the glass surface are replaced by ions of larger radius. This type of exchange should lead to an increase in surface layer volume, which is opposed by the unchanged bulk glass. A compressive stress generated at the surface, compensated by tensile stress in the interior. The ion-exchange is realized below the strain point so that the generated stresses cannot be released by viscous flow and remains in the glass permanently. The advantage of the process consists in the use of low temperatures which avoids the risk of the article deformation and nucleation of crystals.

Three processes are of very importance in practice: replacement of Na^+ ions in glass by K^+ or Ag^+ ions, and replacement of Li^+ ions in glass by Na^+ ions. Most chemical strengthening in commercial use involves the substitution of large ions for small. Such substitution can be effected in two ways: by diffusion and by electrically driven ion migration.

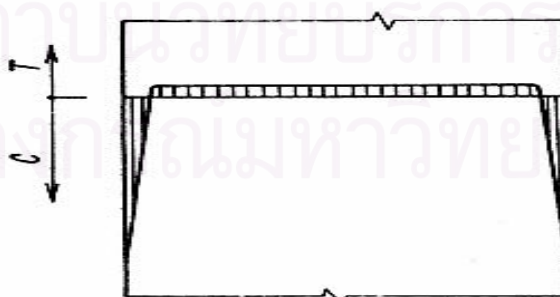


Fig. 2.3. Stress distribution in the wall of a glass object strengthened by ion-exchange.

From Fig. 2.3 the compressive surface layer in ion-exchange glass is much thinner than the tempered glass and the stress at the surface decreases rapidly with depth. The

tensile stress inside the glass body is very low and nearly constant across the thickness. The thickness of the surface compressive layer depends on the rate of ion-exchange and the duration of the process (the thickness of diffusion layer is proportional to the square root of time). The rate of the exchange thus depends on the individual ions mobility, the glass and bath composition and temperature. The temperature used is generally a compromise between the desired increase in mobility and the undesired stress relaxation. From the practical standpoint, alkali ions are more mobile in aluminosilicates than in silicates but less mobile in the borosilicates. Only the ions of Li, Na, K and Ag exhibit a useful degree of mobility. The other alkali ions, polyvalent ions, and even anions should produce stuffing effects. The ion-exchange is as a rule realized in fused salt baths, although some processes also use gaseous, such as SO_2 or solid agents.

The main advantages of chemical strengthening are: high compressive prestress and thus high strength, possibility of strengthening thin-walled articles as well as objects of complex shape without risk of spontaneous fracture and can be machine articles even after strengthening.

2.4 Layered ceramics with different thermal expansion

Multi-layered ceramic composites have proved to be a powerful route to increase both bending strength and toughness of ceramics. Katsuki et al, have shown that the strength of an alumina sheet with its surface covered with mullite and silica (20 to 40 μm thick) was greater than that of the as-sintered sheet. As the average linear thermal expansion coefficient of mullite is lower than that of alumina, a compressive stress due to thermal expansion mismatch is expected to occur on the surface of the alumina sheet covered with mullite and silica during cooling. Macroscopic residual stresses of multi-layered ceramic laminates, which are caused by thermal expansion mismatch or transformation-induced stresses between the layers, are capable of suppressing crack propagation due to a residual compressive stress field around the crack tip [2, 3, 9, 10].

Adachi et al, have studied about nanocomposite materials, in which multi-layered and nanocomposite structure coexisted, nano-sized SiC particles are dispersed into Al_2O_3

and 3Y-TZP layers. These nanocomposites have significantly enhanced fracture strength because of nano-sized particles that dispersed into a matrix prevent grain growth (especially abnormal grain growth) of matrix material and lead to finer microstructure, the strength of nanocomposites is thus improved. Therefore, it is expected that strength of a hybrid composite that combines a multi-layered and nanocomposite could be improved due to nano-sized SiC dispersed in the matrix [6, 8, 11, 12, 13, 14, 15].

2.5 Functionally graded materials (FGMs)

Functionally graded materials (FGMs) are new version of composite materials that are microscopically inhomogeneous in unique characterization because the composition and structure vary gradually and continuously from ceramic to ceramic or ceramic to metal. When FGMs are fabricated by the different components of materials and sintered into high temperature, the thermally induced residual stresses are generated during cooling from the sintering temperature and arise from non-uniform shrinkage of processing. Therefore, solving the problem of thermally induced residual stresses is considerably important to optimize the structure of FGMs and are studied by many researchers [16, 17, 18].

Gang Jin and Hideo Awaji [9] tried to solve this problem in multi-layered FGMs of alumina and nickel plates. In this study, a laminated plate theory was used on the FGMs system to analyze the residual and thermal stresses in the multi-layered process. The analytical results indicated that the residual thermal stress distribution could be controlled by adjusting the compositional gradient across the thickness of the FGMs plates and the characteristics of mismatch between ceramics and metal.

Yong-Ho Choa and Koichi Niihara [1] revealed that residual stress caused by the coefficients of thermal expansion (CTE) mismatch could be controlled by dispersing nano-sized particles with much lower CTE into Al_2O_3 and 3Y-TZP layers. The magnitude of the residual stress was dependent on the mismatch of CTE values between layer components. However, the magnitude of residual stress could be controlled by changing respective layer composition with different CTE.

CHAPTER 3

EXPERIMENTAL PROCEDURES

3.1 Experimental Flowchart

The experimental procedure is divided into 4 steps which are shown in the following flowcharts, Fig 3.1(a), 3.1(b), 3.1(c) and 3.1(d).

Step1 Starting powder preparation and selection.

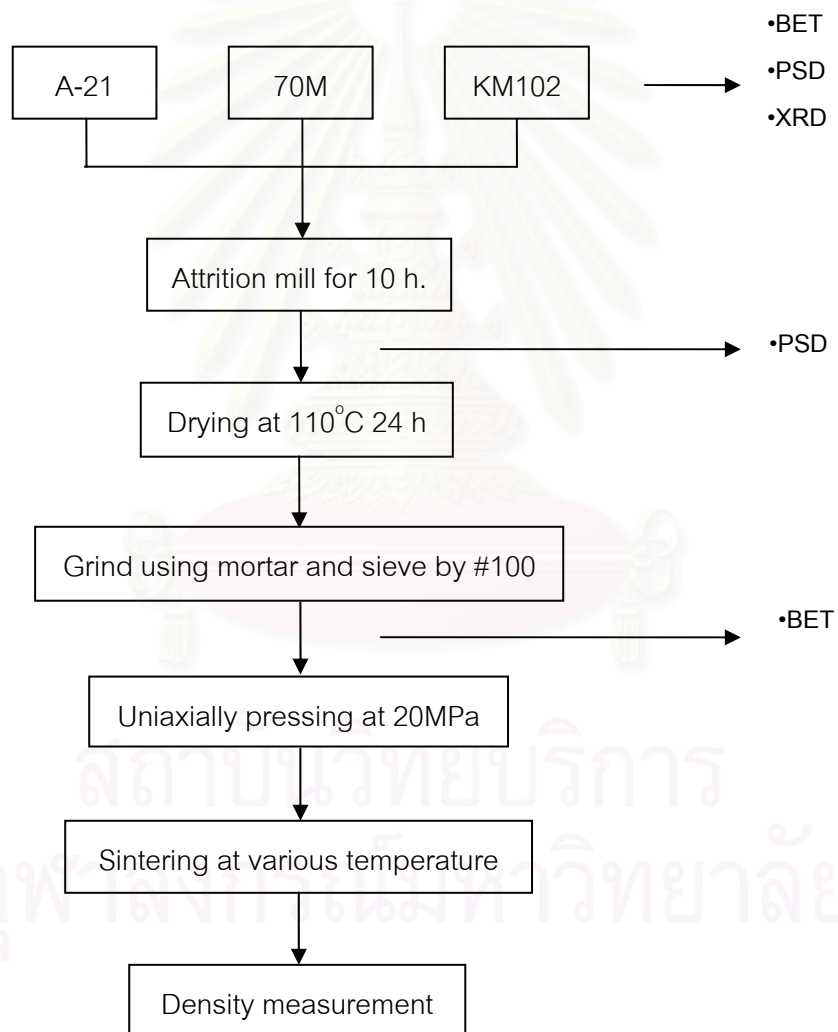


Fig. 3.1(a) Experimental flowchart of starting powder preparation and selection.

Step2 2-layered pellet composite preparation.

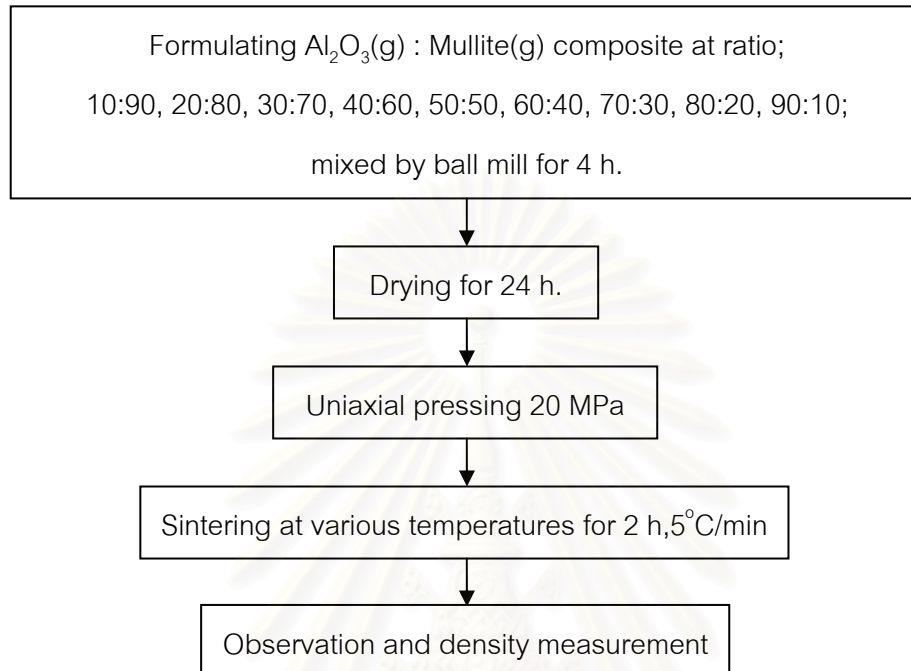


Fig. 3.1(b) Experimental flowchart, step2, 2-layered pellet composites preparation.

สถาบันวิทยบริการ
จุฬาลงกรณ์มหาวิทยาลัย

Step3 Slip casting preparation.

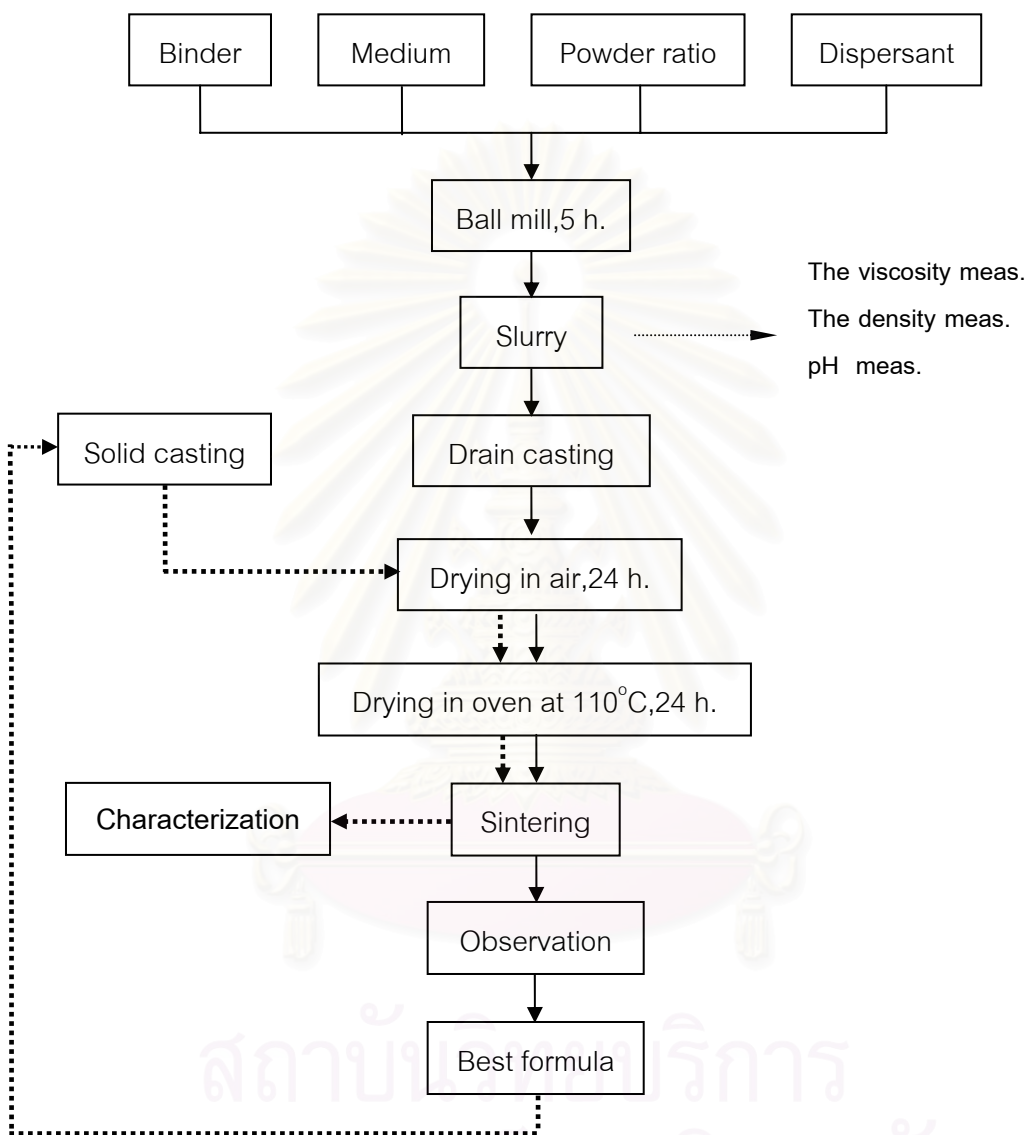


Fig. 3.1(c) Experimental flowchart, step3, slip casting preparation.

Step4 Characterization of slip cast specimens

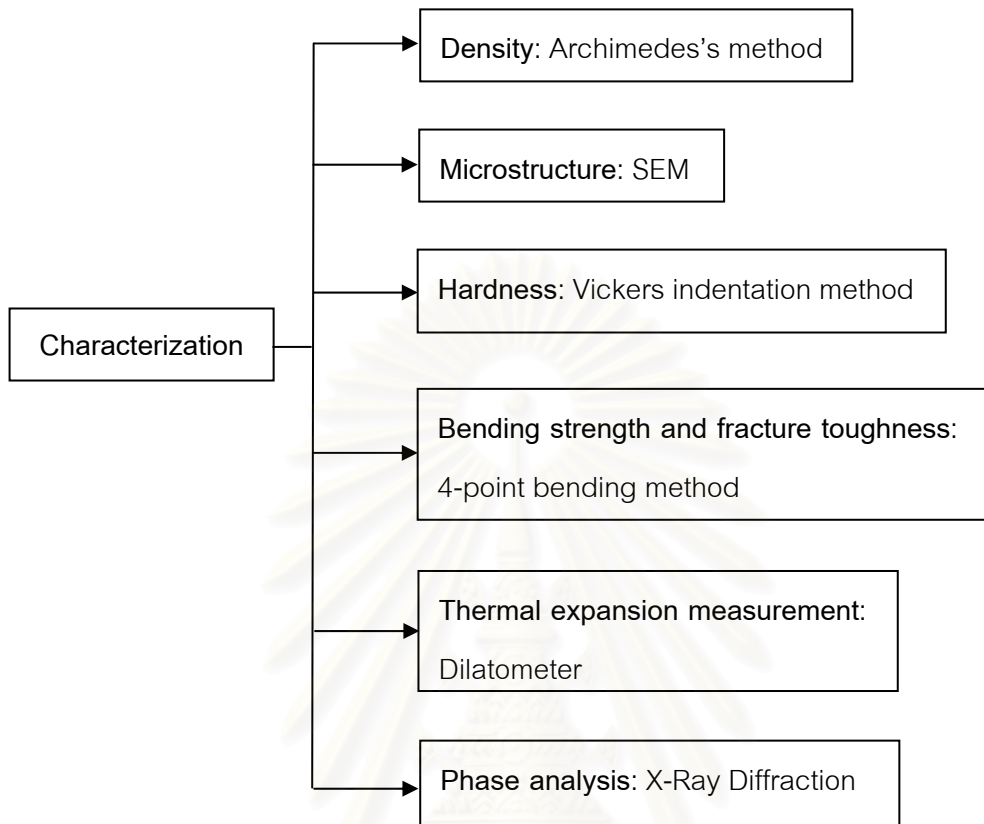


Fig. 3.1(d) Experimental flowchart, step4 characterization.

3.2 Raw materials and characterizations

3.2.1 Raw materials

As the starting materials, alumina A-21 (Sumitomo chemicals, Tokyo, Japan) and 2 different kinds of mullite powder were used for this experiment.

1. 70M from TAIHEIYORUNDUM CO.,Ltd.
2. KM102 from KYORITU MATERIAL CO.,Ltd.

Typical properties received from suppliers for A-21, 70M and KM102 are shown in Table 3.1 and 3.2, respectively.

Table 3.1 Typical properties of alumina A-21.

| Chemical composition and properties | Data |
|--|--------|
| H ₂ O | 0.04 % |
| L.O.I | 0.05 % |
| Fe ₂ O ₃ | 0.01 % |
| SiO ₂ | 0.01 % |
| Na ₂ O | 0.25 % |
| Al ₂ O ₃ | 99.6 % |
| True specific gravity (g/cm ³) | 3.95 |
| Loosed bulk density (g/cm ³) | 0.09 |
| Packed bulk density (g/cm ³) | 1.2 |
| Size of α -crystal (μ m) | 2-4 |
| Linear shrinkage (%) | 16 |
| Mean particle size (μ m) | 50 |

Table 3.2 Typical properties of mullite KM102 and 70M.

| Chemical composition and properties | Data | |
|-------------------------------------|-------|-------|
| | KM102 | 70M |
| SiO ₂ | 27.8 | 23.6 |
| Al ₂ O ₃ | 71.7 | 75.9 |
| Fe ₂ O ₃ | 0.021 | 0.020 |
| TiO ₂ | 0.004 | - |
| CaO | 0.010 | - |
| MgO | 0.022 | - |
| Na ₂ O | 0.019 | 0.080 |
| K ₂ O | 0.003 | - |
| ZrO ₂ | 0.198 | - |
| L.O.I. | 0.42 | - |
| SSA (m ² /g) | 8.7 | - |
| D ₅₀ (μ m) | 0.75 | 2.30 |

3.2.2 Raw materials characterization

3.2.2.1 Particle size distribution

Particle size distributions of alumina A-21, mullite 70M and KM102 were analyzed using sedimentation method by Shimadzu SA-CP2. The measurement was made in the centrifugal sedimentation mode. Furthermore, the particle size of raw powders and milled powders were measured using Master size, Sver.2.18, Malvern Instrument.,Ltd., to ensure the sizes.

3.2.2.2 Specific Surface Area

Specific surface area was measured by BET (Brunauer, Emmett and Teller) method. The sample powders were dried in an oven for 24 h. About 0.2 gram of powder was put in a specific cylinder tube of COULTER SA 3100 surface area and pore size analyzer.

3.2.2.3 X-ray Diffraction Analysis

Raw materials were analyzed by x-ray diffractometer (Bruker D8 Advance) to identify phase of starting materials. The conditions were as follows; 2θ : from 15° - 80° , scanning speed: 0.1/second, anode: Cu, voltage: 40 KV and 30 mA.

3.3 Compositions and preparations of Alumina-mullite composite powder

The compositions of the Alumina-mullite composite were varied from 100 wt% Al_2O_3 to 0 wt% Al_2O_3 as shown in Table 3.3

Table 3.3 Compositions of the Alumina-mullite composite.

| Group of powder milled 10 h | Weight ratio of Alumina and Mullite | | | | | | | | | |
|---|-------------------------------------|----|----|----|----|----|----|----|----|-----|
| | 100 | 90 | 80 | 70 | 60 | 40 | 30 | 20 | 10 | 0 |
| Al_2O_3 A-21 (wt%) (Top layer) | 100 | 90 | 80 | 70 | 60 | 40 | 30 | 20 | 10 | 0 |
| Mullite KM102 (wt%) (Bottom layer) | 0 | 10 | 20 | 30 | 40 | 60 | 70 | 80 | 90 | 100 |

The composites were prepared using ball mill. Alumina A-21 and Mullite KM102 were separately milled for 10 h as the starting powder. The milled powders were wet mixed in a polypropylene bottle (250 cm³) for 4 h. The slurry was dried at 110 °C for 24 h in an oven to remove water. The dry milled powders were mixed with 1.0 wt% of polyvinyl alcohol (PVA 10000-15000 MW, 13 grams of polyvinyl alcohol to 87 grams of water) as binder and sieved through a 100 mesh screen. Then, 3 grams of each powder was pressed into 2-layered pellets of 20 mm in diameter by uniaxial press at the pressure of 20 MPa. All specimens were dried at 110 °C to remove humidity. After that the specimens were sintered at 1400, 1500, 1600, 1650, 1700 °C with a heating and a cooling rate of 5 °C/m and kept for 2 h. Then the densities of all sintered specimens were measured by Archimedes's method.

3.4 Slip casting conditions of Alumina-mullite 2-layered tube and composite plate

The compositions of alumina and mullite slurries for slip casting of tube and plate are shown in Table 3.4

These compositions (60 wt% of solid loading) were mixed by ball-milled (polypropylene bottle and Al₂O₃ balls) for 5 h. with 0.7 wt% of Dispex N-40 as a dispersant and 1 wt% of CMC as a binder in a medium solution of distilled water. After milling, these slurries were filtered and ultrasonicated for 5 min.

The 1st composition (bottom) was poured into the gypsum mold and kept 30 min. After that, the 2nd composition (top) was poured followed by the same 30 min keeping.

The best composite was selected to study about the basic properties of each separate layer. Solid casting process was used in the case of plate specimen and hollow ware casting process was used for tube specimen.

Table 3.4 Compositions of alumina and mullite slurries to fabricated 2-layered tube composite.

| Process 1 | Weight ratio of Alumina and Mullite(A:M) | | | | |
|------------------------------|--|-------|-------|-------|-------|
| 1 st layer(outer) | 100:0 | 90:10 | 80:20 | 70:30 | 60:40 |
| 2 nd layer(inner) | 0:100 | 10:90 | 20:80 | 30:70 | 40:60 |

| Process 2 | Weight ratio of Alumina and Mullite(A:M) | | | | |
|------------------------------|--|-------|-------|-------|-------|
| 1 st layer(inner) | 100:0 | 90:10 | 80:20 | 70:30 | 60:40 |
| 2 nd layer(outer) | 0:100 | 10:90 | 20:80 | 30:70 | 40:60 |

3.5 Characterization of sintered specimens

3.5.1 Shrinkage

The sizes of specimens were measured by vernier caliper.

Shrinkage of sintered specimens and after firing was calculated by the equation (3.1) and (3.2).

$$\% \text{ Linear shrinkage} = \left[\frac{L_g}{L_g - L_f} \right] \times 100 \dots\dots\dots (3.1)$$

$$\% \text{ Volume shrinkage} = \left[\frac{V_g}{V_g - V_f} \right] \times 100 \dots\dots\dots (3.2)$$

Where;

V_g, L_g = The Volume and Length of green specimen.

V_f, L_f =The Volume and Length of fired specimen.

3.5.2 Bulk density, water absorption and relative density

The bulk density and water absorption of specimens were measured according to Archimedes's method.

Theoretical density of sintered specimens were calculated from the specific gravity of each component using equation (3.3)

$$\text{Theoretical density } (\rho_t) = f_1\rho_1 + f_2\rho_2 \quad \dots\dots\dots (3.3)$$

Where; f = fraction of each component
 ρ = specific gravity of each component
 1, 2,.. = number of component

In this experiment, the theoretical density of mullite = 3.17 g/cm^3
 (ρ_1), $\text{Al}_2\text{O}_3 = 3.95 \text{ g/cm}^3$ (ρ_2) were taken as references.

Using equation (3.3) the theoretical density of each composite was calculated and shown in Table 3.5, and from these values, relative densities were calculated. (0A100M composition; the theoretical density from calculation is about 3.21 g/cm^3 caused from the contamination of Al_2O_3 balls during the powder preparation process.)

Table 3.5 Theoretical density of each composite from calculation

| Composition | Theoretical density (g/cm^3) |
|-------------|---|
| 100A 0M | 3.95 |
| 90A 10M | 3.88 |
| 80A 20M | 3.80 |
| 70A 30M | 3.73 |
| 60A 40M | 3.65 |
| 50A 50M | 3.58 |
| 40A 60M | 3.50 |
| 30A 70M | 3.43 |
| 20A 80M | 3.36 |
| 90A 10M | 3.28 |
| 0A 100M | 3.21 |

3.5.3 Observation of microstructure by scanning electron microscope (SEM)

The microstructures of sintered specimens were examined by a scanning electron microscope (SEM) (JEOL: JSM-5410L). The specimens were polished with silicon carbide powders, grit No.2000 and 8000, on a glass plate. After polishing, specimens were thermally etched at 1500°C for 30 min, followed by gold sputtering.

The procedure of sample preparation is shown in Fig 3.2

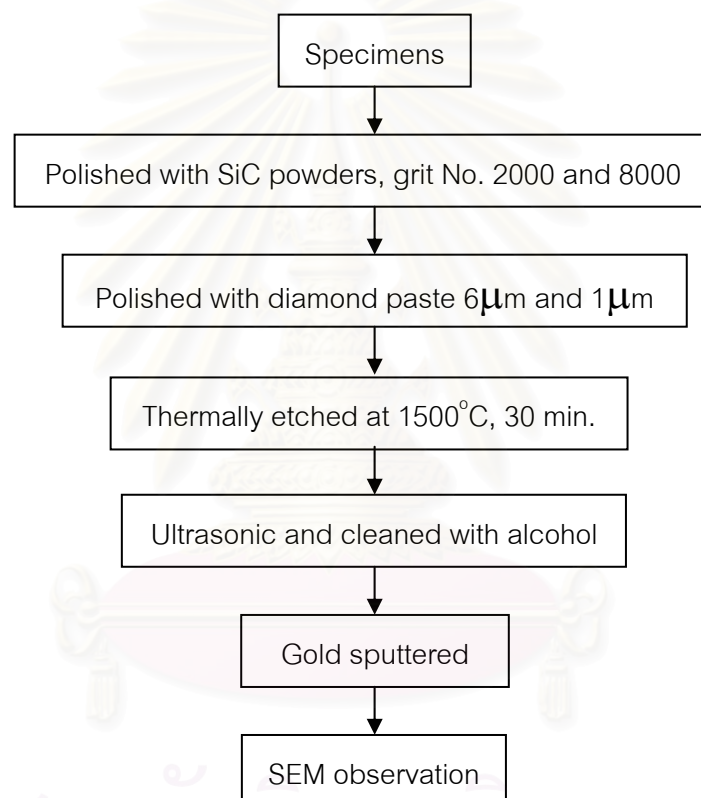


Fig. 3.2. Flow chart of sample preparation for SEM observation

3.5.4 Vickers hardness and fracture toughness measurement

The Vickers indentation method with a load of 10 Kg (98.07N), (Microhardness Tester Model Zwick I), was used to measure both the hardness and toughness.

Vickers hardness (H_v) was calculated by the eqn. (3.7) (JIS R160 – 1991)

$$H_v = 1.8544 \times \frac{P}{(2a)^2} \dots\dots\dots (3.7)$$

where; P = load (N)

a = length of diagonal (m)

Fracture toughness (K_{IC}) was calculated by the eqn. (3.8) (JIS R1607 – 1995)

$$K_{IC} = 0.018(E/Hv)^{1/2} (P/C^{3/2}) \dots\dots\dots (3.8)$$

Where; E = elastic modulus (Pa)

C = crack length (m)

3.5.5 Strength and Young's modulus measurement

The strength and Young's modulus of specimens were measured by 4- point bending method, in conformity with JIS standard R1601-1995. One 4x40 mm face of a rectangular specimen of the size 3x4x40 mm was polished on the glass plate with silicon carbide powders, grit No 2000 for 20 min and No 8000 for 30 min. Both edges of 40 mm length were cut about 0.5 mm at 45° to remove cracks in the edges.

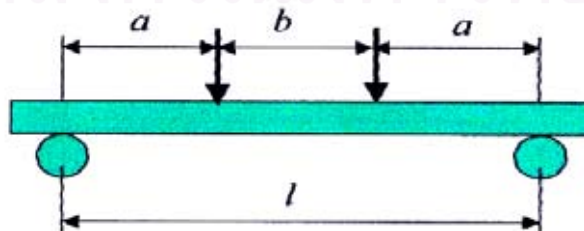


Fig. 3.3. Schematically of 4-point bending test

Bending strength (σ_{b4}) was calculated by the eqn. (3.9)(JIS R1602-1995)

$$\begin{aligned}\sigma_{b4} &= \frac{3P}{2dh^2} (l-a) \\ &= \frac{P.l}{dh^2} \dots\dots\dots (3.9)\end{aligned}$$

Where; d=width (m) and h= thickness (m) of specimens, l= span length (m).

Young's modulus (E) was also calculated by the eqn. (3.10)(JIS R1602-1995)

$$E = \frac{23P.l^3}{108V_{\max}dh^3} \dots\dots\dots (3.10)$$

Where; V_{\max} is the displacement of specimen.

สถาบันวิทยบริการ
จุฬาลงกรณ์มหาวิทยาลัย

CHAPTER 4

EXPERIMENTAL RESULTS AND DISCUSSION

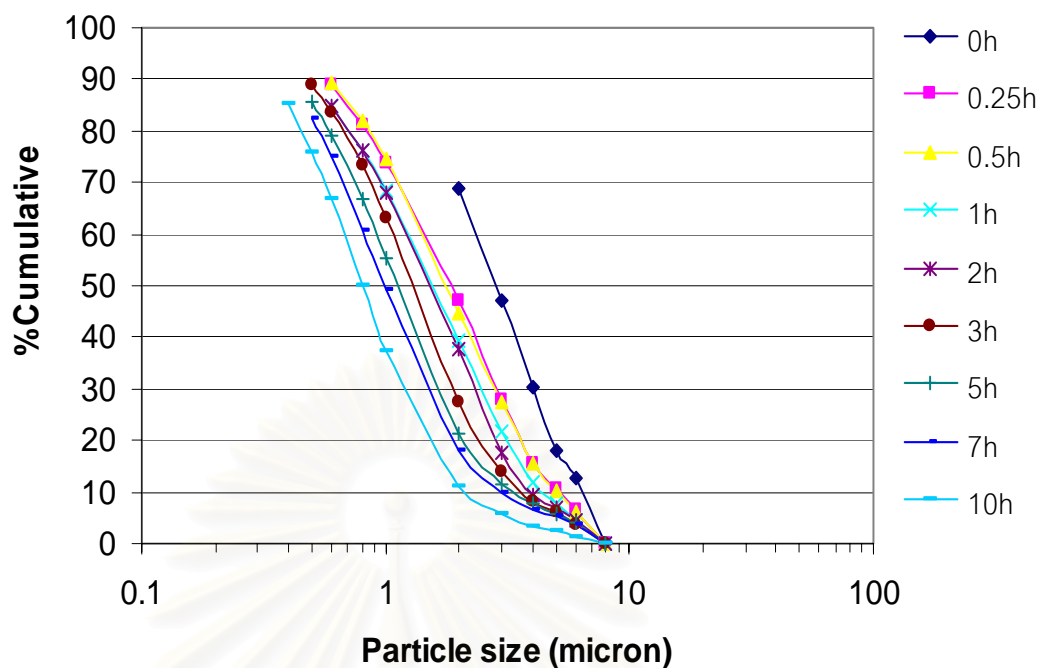
4.1 Raw material characterization

4.1.1 Particle size distribution

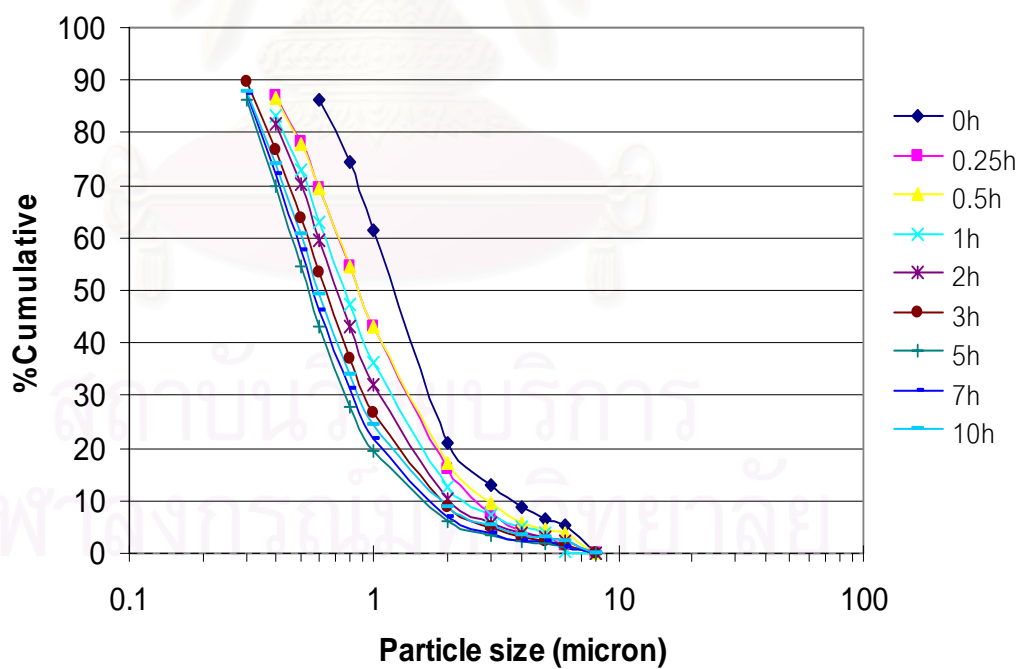
Particle size distributions of two types of raw mullite material, 70M and KM102, are shown in Fig. 4.1. The average particle size value ($0.53 \mu\text{m}$) of KM102 is smaller than that ($0.64 \mu\text{m}$) of 70M, both milled for 10 h with attrition mill. The accumulated curve and histogram of the particle milled for 10 h are shown in Fig. 4.2. Particle size distribution of KM102 (Fig. 4.2(b)) shows narrow distribution curve than 70M.



สถาบันวิทยบริการ
จุฬาลงกรณ์มหาวิทยาลัย

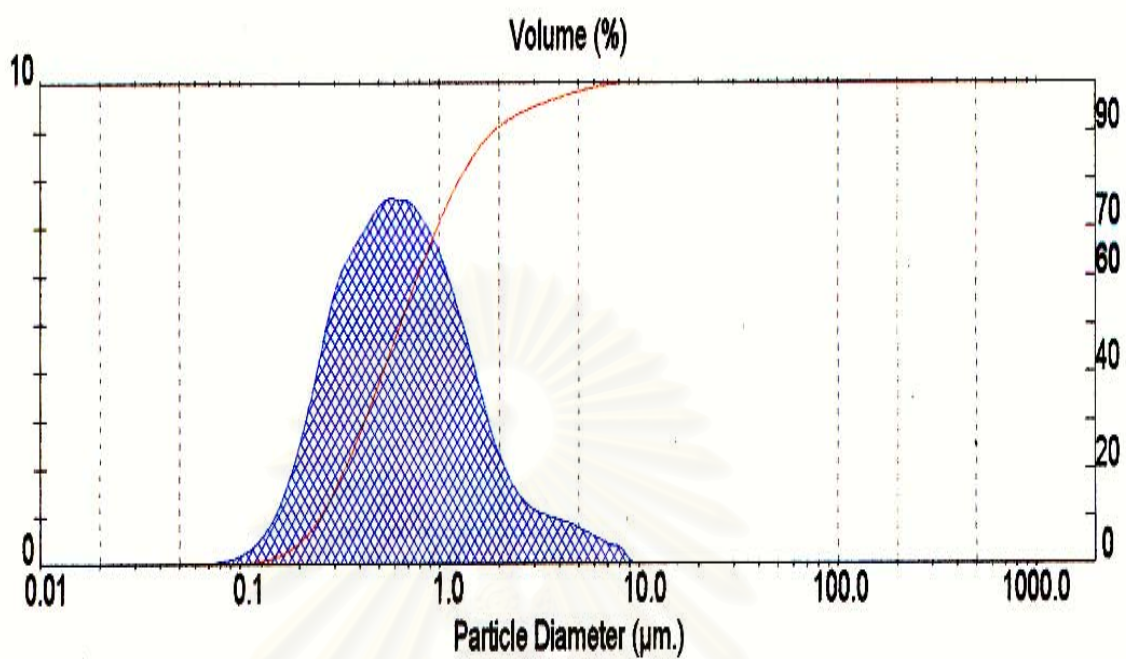


(a)

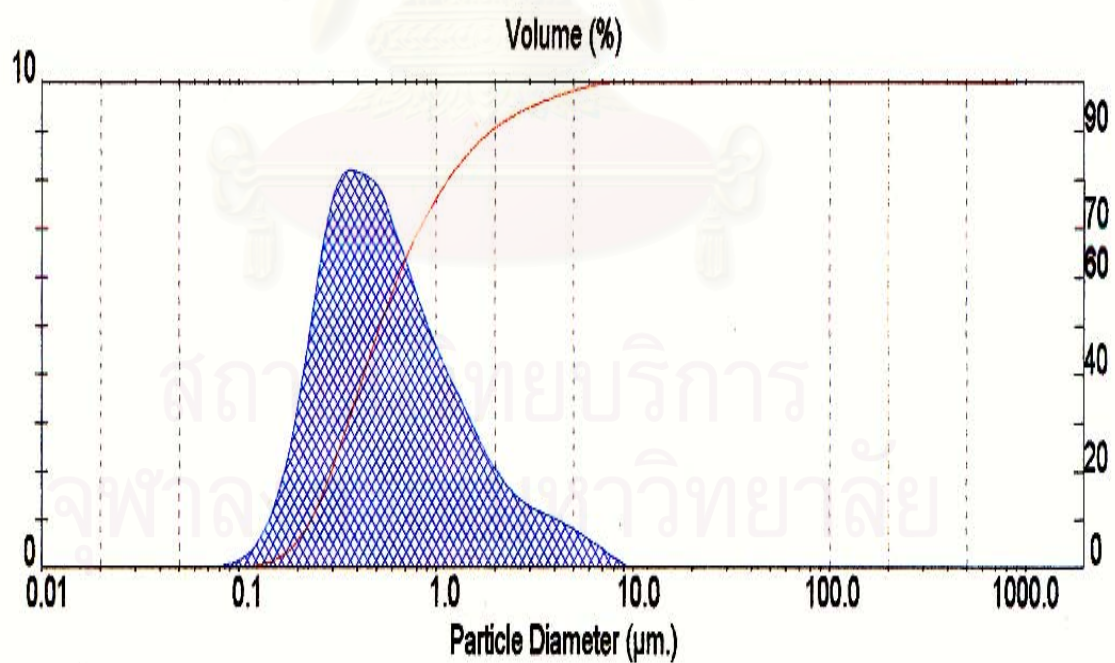


(b)

Fig. 4.1. Particle size distribution of mullite 70M (a) and mullite KM102 (b) sampling at various periods of milling time.



(a)



(b)

Fig. 4.2. Particle size distribution of mullite 70M (a) and mullite KM102 (b) milled 10h with alumina balls.

4.1.2 Specific surface area

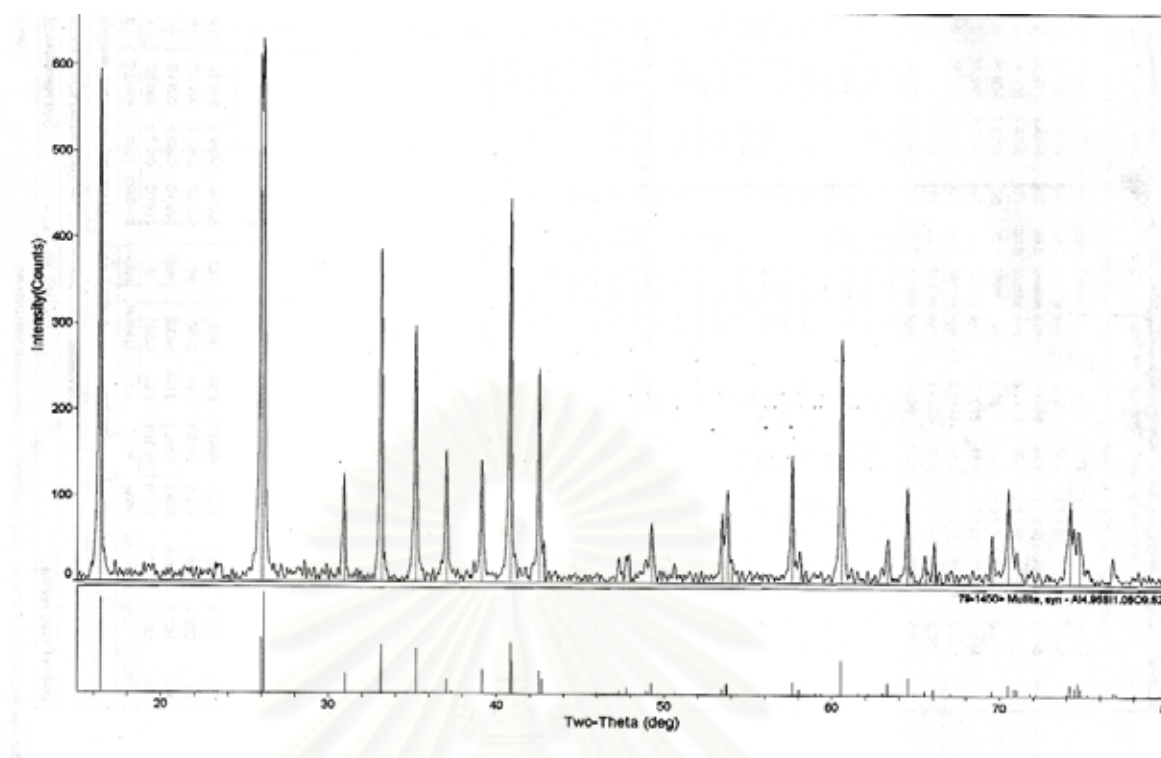
Table 4.1 shows the values of specific surface area (SSA) of raw materials, the value of SSA before milling was low and increasing after milling with Attrition mill for 10 h. After milling, the SSA of 70M (25.8 m²/g) was larger than that of KM102 (14.0 m²/g). However, the average particle size of 70M (0.64 μ m) was larger than that of KM102 (0.53 μ m). This difference can not be explained from the data.

Table 4.1. Specific surface area of powders

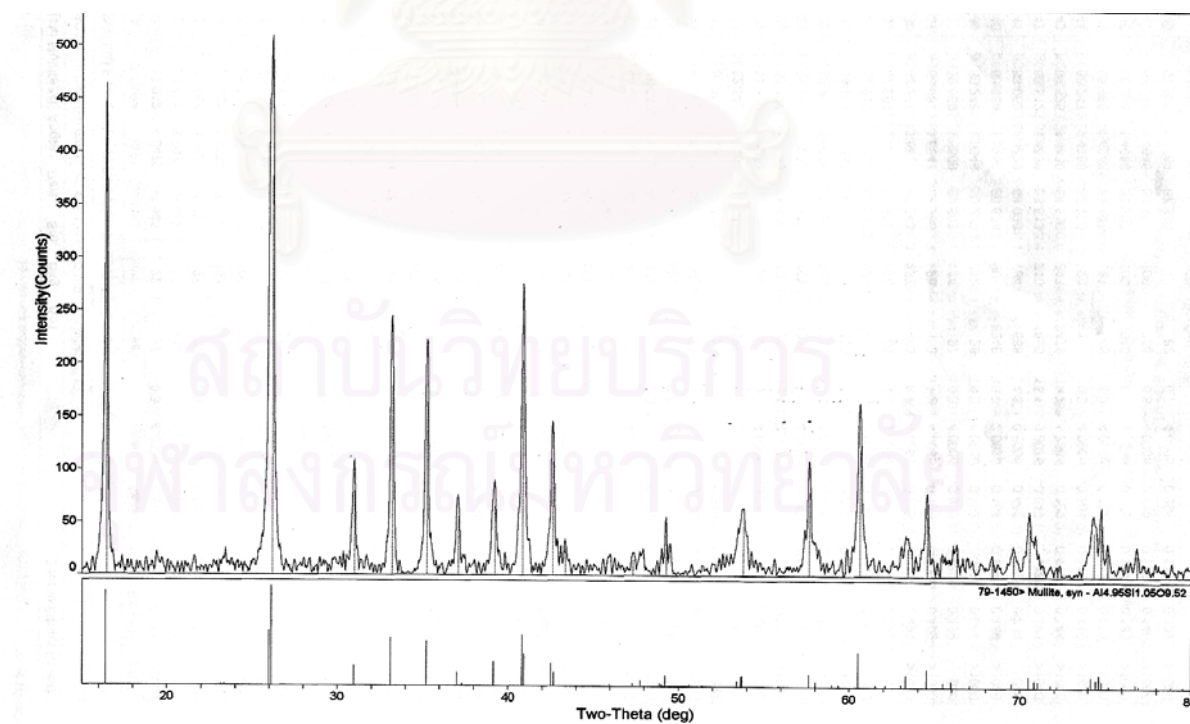
| Starting materials(Commercial grade) | SSA(m ² /g) | |
|--------------------------------------|------------------------|-----------------------|
| | Raw | Attrition milled 10 h |
| Alumina (A-21) | 0.87 | 11.5 |
| Mullite (70M) | 2.74 | 25.8 |
| Mullite (KM102) | 8.26 | 14.0 |

4.1.3 X-Ray diffraction analysis

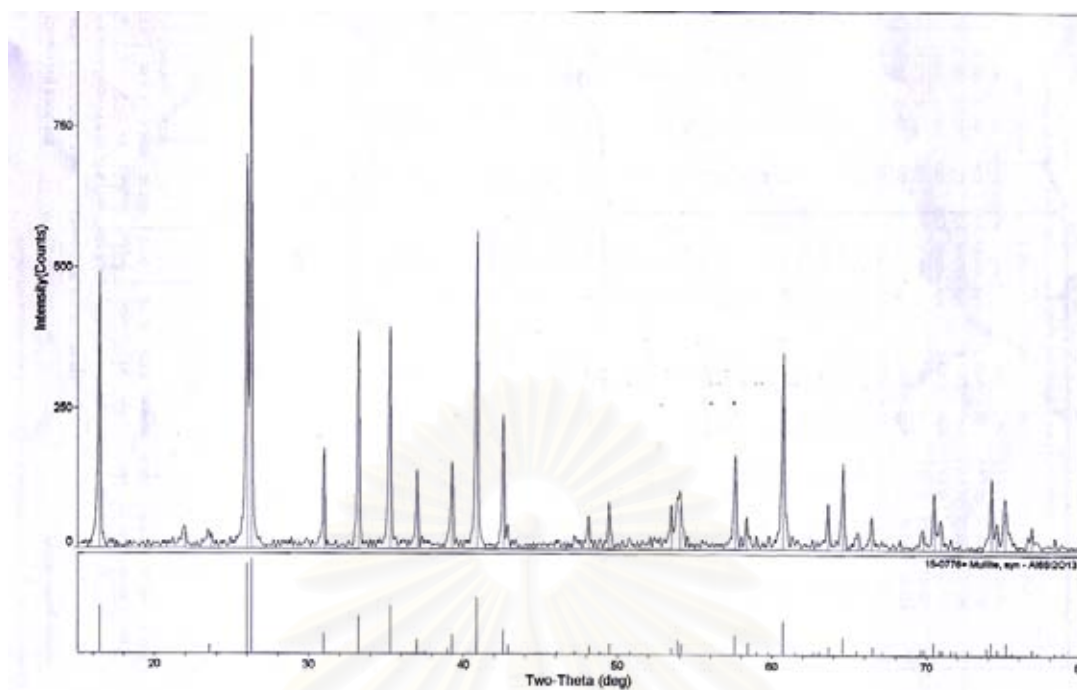
X-Ray diffraction profiles of mullite 70M and KM102 before and after milling are the same. After milling of mullite powders for 10 hours by Al₂O₃ balls, wear of balls are about 4.97% and 4.47% for 70M and KM102, respectively. However, no Al₂O₃ peak was observed in fig.4.3 (b) and (d).



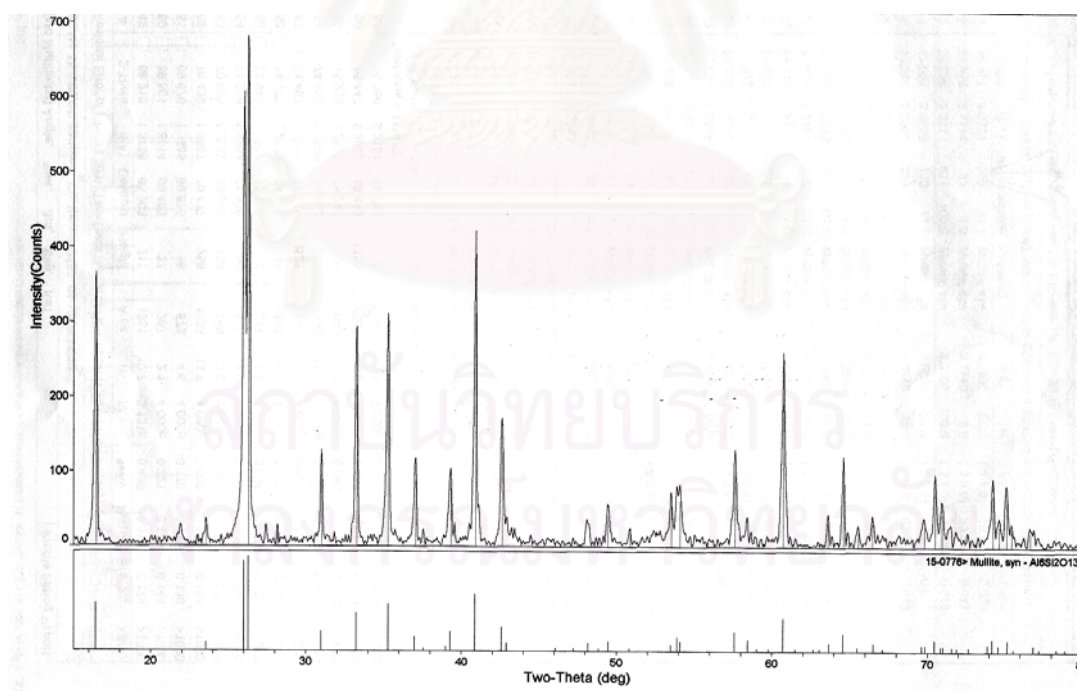
(a) Raw mullite 70M



(b) 70M milled 10 h



(c) Raw mullite KM102

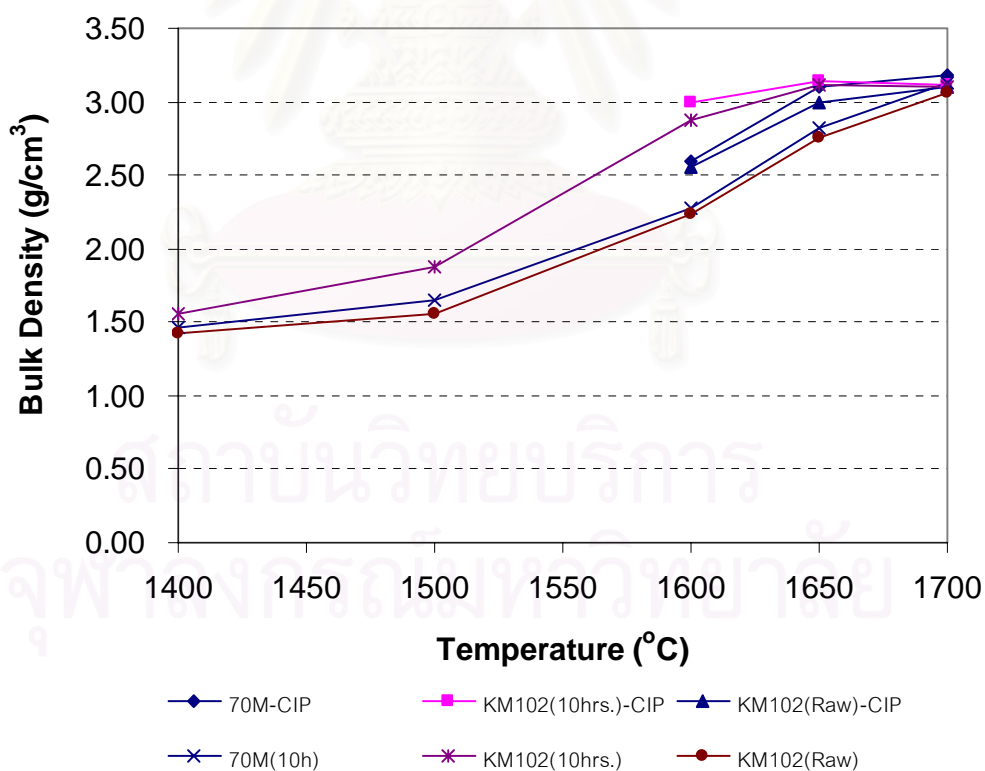


(d) KM102 milled 10 h

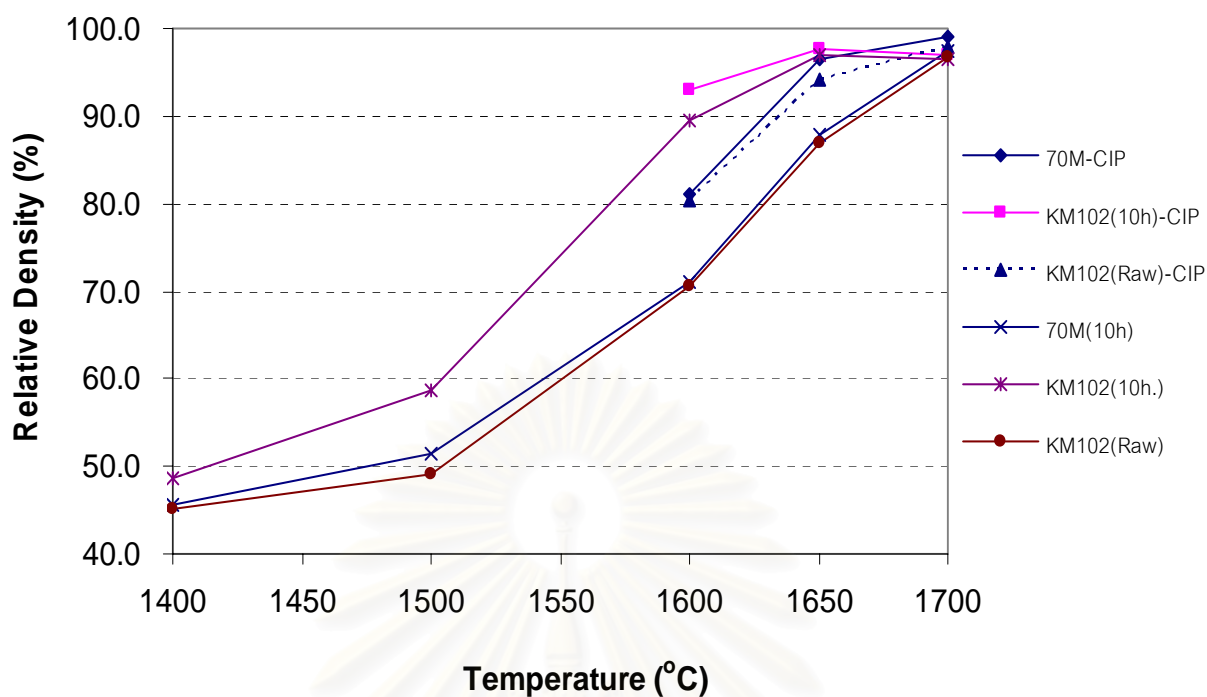
Fig. 4.3. X-Ray diffraction patterns of raw mullite (a)70M, (b)70M milled 10 h, (c) raw mullite KM102 and (d) KM102 milled 10 h.

4.2 Preliminary sintering of Alumina and mullite

The bulk densities of both mullites sintered at various temperatures are shown in Fig. 4.4(a). The bulk density of 70M after milled for 10 hours was close to the value of the as received KM 102 and the value reached maximum at 1700 °C. While KM 102 after milling for 10 hours showed higher density at all temperatures and the maximum density was observed at 1650 °C. Moreover, the bulk density of KM 102 after milling for 10 hours did not change by applying CIP. When considering the volume shrinkage shown in Fig 4.5, higher volume shrinkage specimens showed higher density. As shown in Fig 4.5, A-21 shrank more than any mullite at lower temperature range of 1400-1500 °C. However, the shrinkage became similar at the temperature range of 1600-1700 °C.



(a)



(b)

Fig. 4.4. Relationship between (a) bulk density and (b) relative density with temperature for various starting materials.

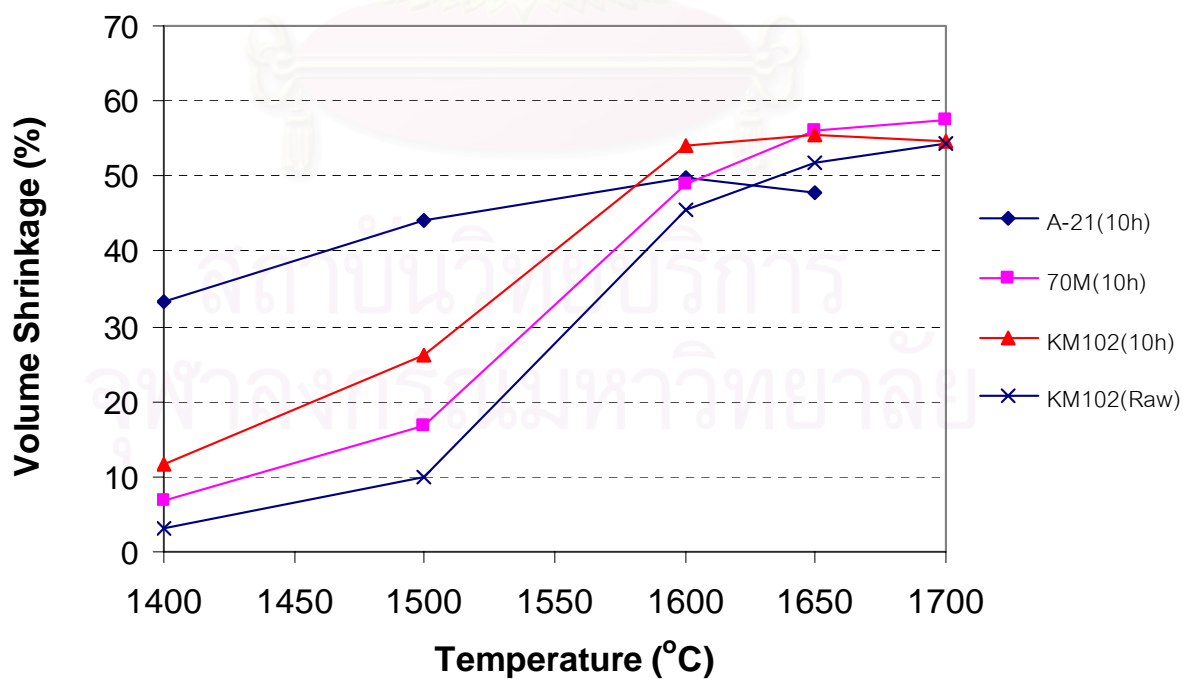


Fig. 4.5. Volume shrinkage of starting materials at various temperatures.

4.3 Sintering a 2-layered pellet formed by die pressing

From the data shown in Fig 4.4 and 4.5, KM102 (10h) was selected as the mullite powder used for the following experiments. The multi-layered pellets were formed by die pressing. The composition of 2-layered composite pellet was changed from 100A/100M to 60A40M/40A60M as shown in Table 4.2. As seen in Table 4.2, most specimens cracked vertically and horizontally. The fractures were more serious when the composition difference was big. The extent of rough surface and smooth surface between the interfaces did not affect the fracture. 3-layered of components, which composed of the buffer layer, was fabricated as shown in Table 4.3. However, the same result was found in this specimen too. It was also found that the specimen with composition 60A40M/40A60M could be sintered without any cracking. Bulk density of this specimen was about 3.45 g/cm^3 .

Delamination was also occurred randomly near the interface of each component. Cracked specimens were fixed to one body without layer gaps. Therefore, these cracks were generated during cooling by the stress due to the thermal expansion mismatch. Because the stress generates at the edge of diameter and it easily cracks the specimen. From the random delamination of specimens, it was concluded that the multi-layered structure of Al_2O_3 and mullite could not be realized in the pellet form.

The stress occurred in the hybrid layer is simply (roughly) calculated from the following equation.





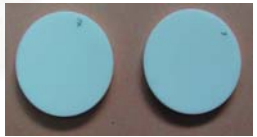
$$\sigma = E \Delta\alpha \Delta T \dots\dots\dots (3.11)$$

σ = Stress E = Young's modulus $\Delta\alpha$ = Thermal expansion difference

ΔT = Temperature difference.

In this experiment, when $E = 300 \text{ GPa}$, $\Delta\alpha = 3.8 \times 10^{-6} \text{ }^\circ\text{C}^{-1}$ and $\Delta T = 1500 \text{ }^\circ\text{C}$, σ is calculated as 1700 MPa . When $E = 250 \text{ GPa}$, $\Delta\alpha = 0.7 \times 10^{-6} \text{ }^\circ\text{C}^{-1}$ and $\Delta T = 1500 \text{ }^\circ\text{C}$, σ is about 260 MPa . From these values, it is understood that 100A/100M was broken. And some of specimen with 60A40M/40A60M composition was sound.


Table 4.2. Pictures of 2- layered pellet specimens, formed by die pressing and sintered at 1650 °C 2 h.

| A-21 : KM102 (wt%) | | Interface | | Observations |
|-------------------------|----------------|-----------|--------|---|
| (Top layer) | (Bottom layer) | Rough | Smooth | |
| 100:0 | 0:100 | | ✓ |  |
| 90:10 | 10:90 | ✓ | ✓ |  |
| 80:20 | 20:80 | ✓ | ✓ |  |
| 70:30 | 30:70 | ✓ | ✓ |  |
| 60:40 | 40:60 | ✓ | ✓ |  Bulk den.=3.45 g/cm ³ |

Rough: After KM102 pressed, the surface was scratched to make the surface rough. And then A-21 powder was set and pressed.

Smooth: After KM102 pressed, A-21 powder was supplied on the pressed surface and pressed.

Table 4.3. Picture of 3-layered pellet specimen formed by die pressing and sintered at 1650 °C for 2 h.

| Components | Weight ratio of Alumina and Mullite (A:M) | Observations |
|-----------------------|---|--|
| 1 st layer | 30:70 |  |
| 2 nd layer | 50:50 | |
| 3 rd layer | 70:30 | |

4.4 Sintering a 2-layered tube formed by slip casting

From the result of 2-layered pellet composite specimens formed by die pressing, we thought that there was no edge at which stress concentrate, when the figure was tube. The slip cast of 2-layered tube specimens were fabricated.

Table 4.4 and 4.5, show slip cast and sintered tube specimens. In process 1 (Table 4.4), inner layer is mainly mullite and outer layer is mainly Al_2O_3 . In process 2 (Table 4.5), the arrangement is in reverse. That is, on the process 1, tensile stress generates in outer layer and compressive stress generates in the outer layer on the process 2 [2, 3].

After the specimens sintered at 1650 °C, 2h, with a heating rate of 5 °C/min, all specimens in process 1 were completely broken in the vertical direction, as shown in Table 4.4. On the other hand, in process 2 one composition of composite was not broken, that one is the specimen with 40A60M in outer layer and 60A40M in inner layer. As shown in Table 4.5. Bulk density of this specimen was about 3.57 g/cm³. As a result, it was concluded that this kind of multi-layered composite with different of the coefficients of thermal expansion will be applicable to practical applications when the thermal expansion difference is smaller than the case of 40A60M /60A40M.

Table 4.4. Picture of 2-layered tube specimens (Process 1) formed by slip casting and sintered at 1650 °C for 2h.




| Process 1 | Weight ratio of Alumina and Mullite(A:M) | | | | |
|------------------------------|--|-------|-------|-------|-------|
| 1 st layer(outer) | 100:0 | 90:10 | 80:20 | 70:30 | 60:40 |
| 2 nd layer(inner) | 0:100 | 10:90 | 20:80 | 30:70 | 40:60 |
| Observations |  | | | | |

Table 4.5. Picture of 2-layered tube specimens (Process 2), formed by slip casting and sintered at 1650 °C for 2h.

| Process 2 | Weight ratio of Alumina and Mullite(A:M) | | | | |
|------------------------------|---|-------|--|-------|-------|
| 1 st layer(inner) | 100:0 | 90:10 | 80:20 | 70:30 | 60:40 |
| 2 nd layer(outer) | 0:100 | 10:90 | 20:80 | 30:70 | 40:60 |
| Observations |  | |  <p>Bulk den.=3.57g/cm³</p> | | |

4.5 Characterization of sintered ceramics

4.5.1 Shrinkage

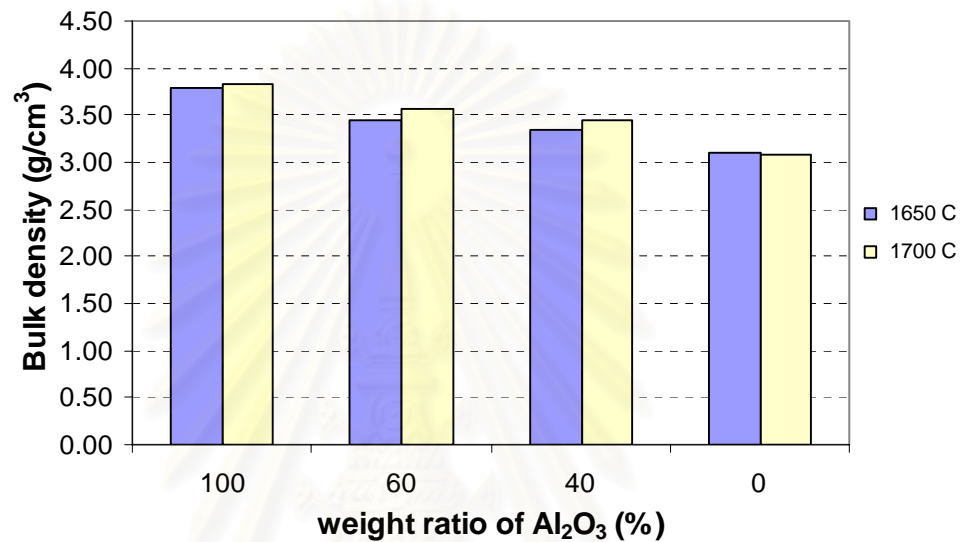
The linear shrinkage and the volume shrinkage of specimens are about 20% and 50%, respectively

Table 4.6. Volume shrinkage and Linear shrinkage of specimens sintered at 1650 °C for 2h.

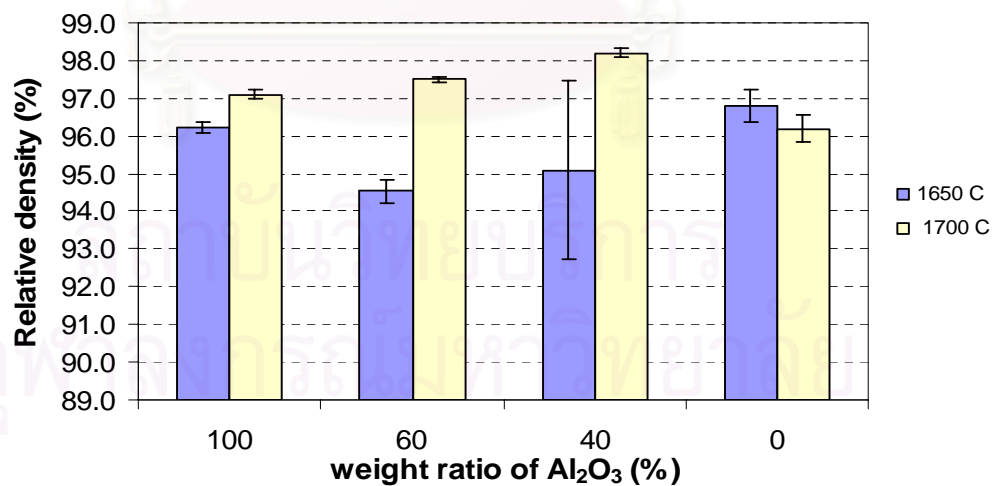
| Fabrication methods | Compositions | Volume Shrinkage (%) | Linear Shrinkage (%) |
|--------------------------|--------------------------------|----------------------|----------------------|
| Pellet(2-layered) | 40A60M(Top) 60A40M(Bottom) | 51.6 | 21.8 |
| Plate (solid casting) | 60A40M | 52.0 | 22.5 |
| | 40A60M | 52.5 | 22.4 |
| Tube (drain casting) | 100A | 51.4 | 21.0 |
| | 100M | 52.7 | 22.0 |
| | 40A60M(outer) 60A40M(inner) | 49.7 | 20.0 |

4.5.2 Bulk density, water absorption and relative density

Fig. 4.6 (a) and (b) show the bulk density and relative density of the specimens formed by slip casting and sintered at 1650, 1700 °C for 2h at a heating rate of 5°C/min. The bulk densities of specimens increase with elevating sintering temperature. All data are shown in the Appendix A (Table A-1 and A-2).



(a)



(b)

Fig. 4.6. Bulk density (a) and relative density (b) of specimens formed by slip casting and sintered at 1650 °C and 1700 °C for 2h at a heating rate of 5°C/min.

Fig. 4.7 shows water absorption. All specimens except 40A60M at 1650°C shows very small water absorption (less than 0.05%).

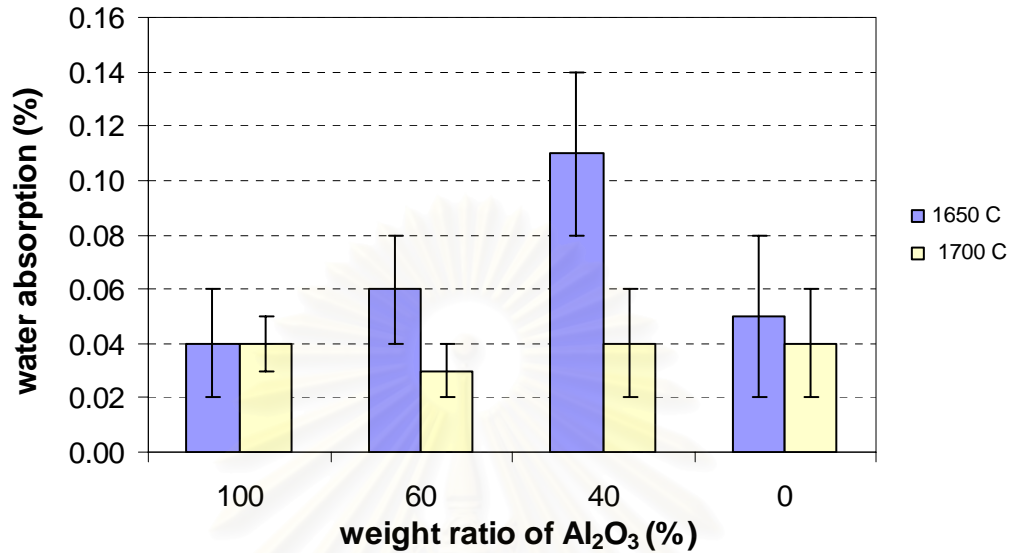
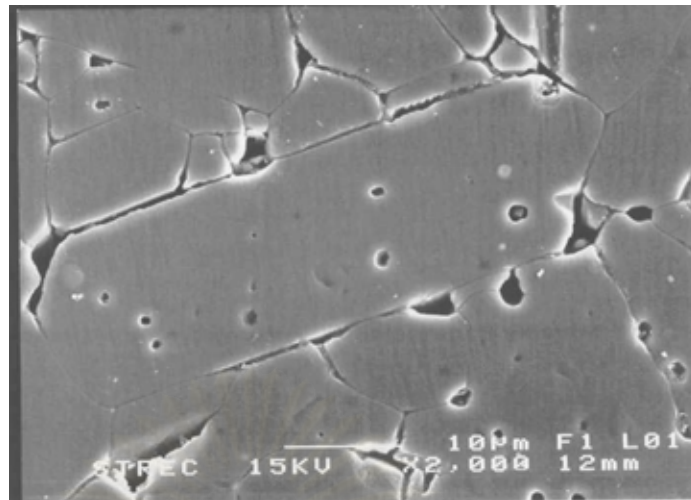


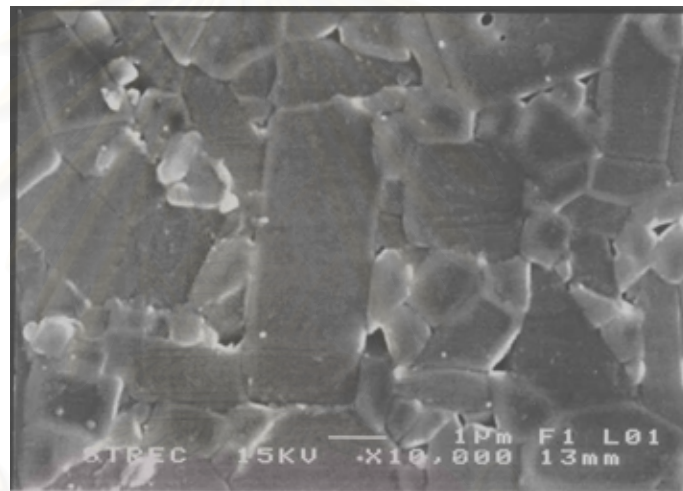
Fig. 4.7. Water absorption of specimens formed by slip casting and sintered at 1650 and 1700 °C for 2h at a heating rate of 5°C/min.

4.5.3 Microstructure of sintered specimen by SEM

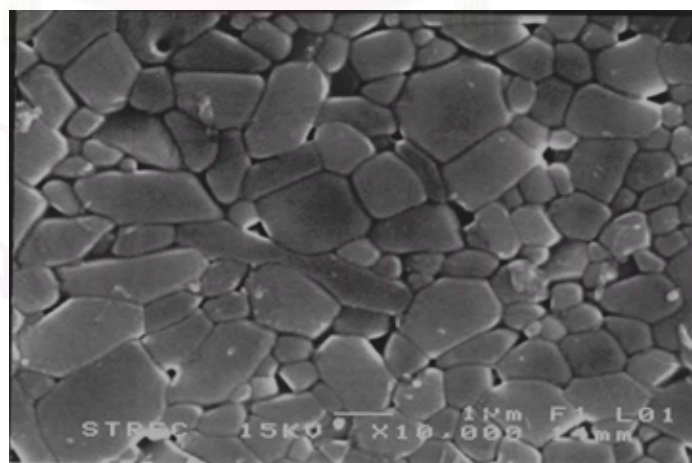
Fig. 4.8 (a), (b), and (c) show the microstructures of pure A-21, pure KM102 and composite of 40A60M sintered at 1700°C for 2 h. Pure A-21 shows an abnormal grain growth. Pure KM102 shows bimodal structure and some of grains have inequiaxial shape. On the other hand, 40A60M composite shows small grain size and equiaxial grain shape, as shown in Fig. 4.8(c).



(a)



(b)



(c)

Fig. 4.8. SEM micrographs of sintered slip cast specimens at 1700 °C, 2 h, (a) A-21, (b) KM102 and (c) composite of 40A60M.

Fig. 4.9 shows the average grain sizes of 100A, 60A40M, 40A60M and 100M sintered at 1650 and 1700 °C for 2 h. Pure Al_2O_3 (100A) sintered at 1700 °C shows the largest average grain size of 11.06 μm . On the contrary, pure mullite sintered at 1650°C shows the smallest average grain size of 1.02 μm . The microstructures of composite specimens, such as 60A40M and 40A60M show small grain size and equiaxial grain shape as shown in Fig. 4.8 (c). Moreover, at higher temperature the composites do not show much grain growth.

The small grain size combined with an equiaxial grain shape of composites was caused by the effect of second phase acted as an inhibitor of grain growth on alumina matrix grain.

Yasuoka et al. [6] reported that the second phase dispersed in a matrix, such as $\text{Al}_2\text{O}_3/\text{LaAl}_{11}\text{O}_{18}$ system, could inhibit the anisotropic grain growth of matrix grain. The presence of $\text{LaAl}_{11}\text{O}_{18}$ platelets acted as inhibitor and remained equiaxial grain shape of the matrix.

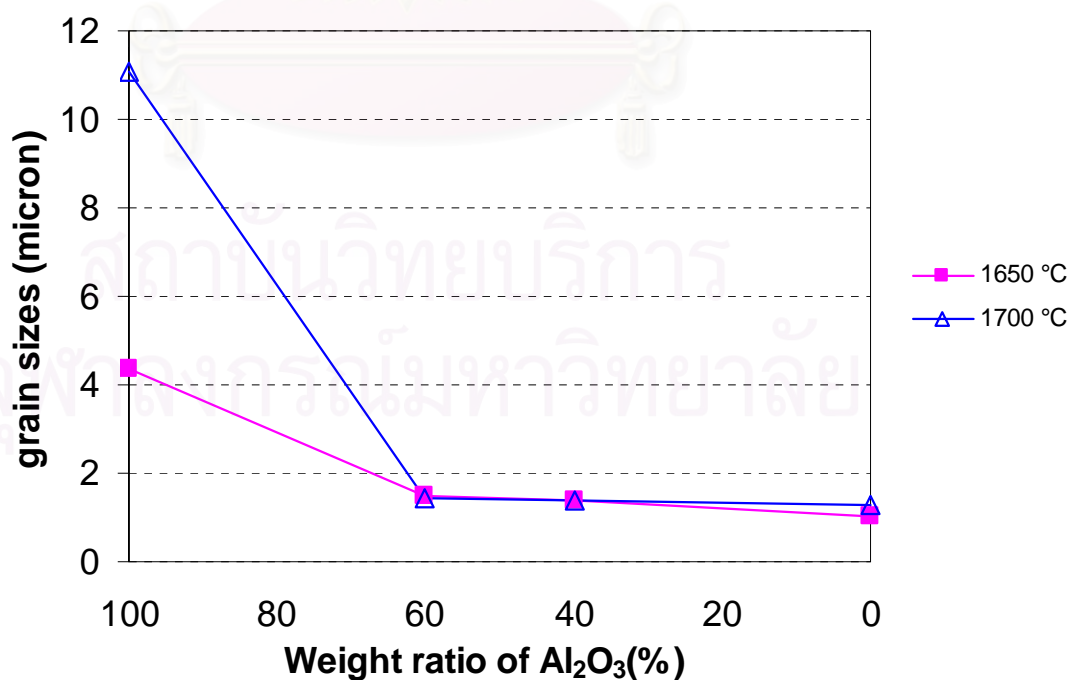


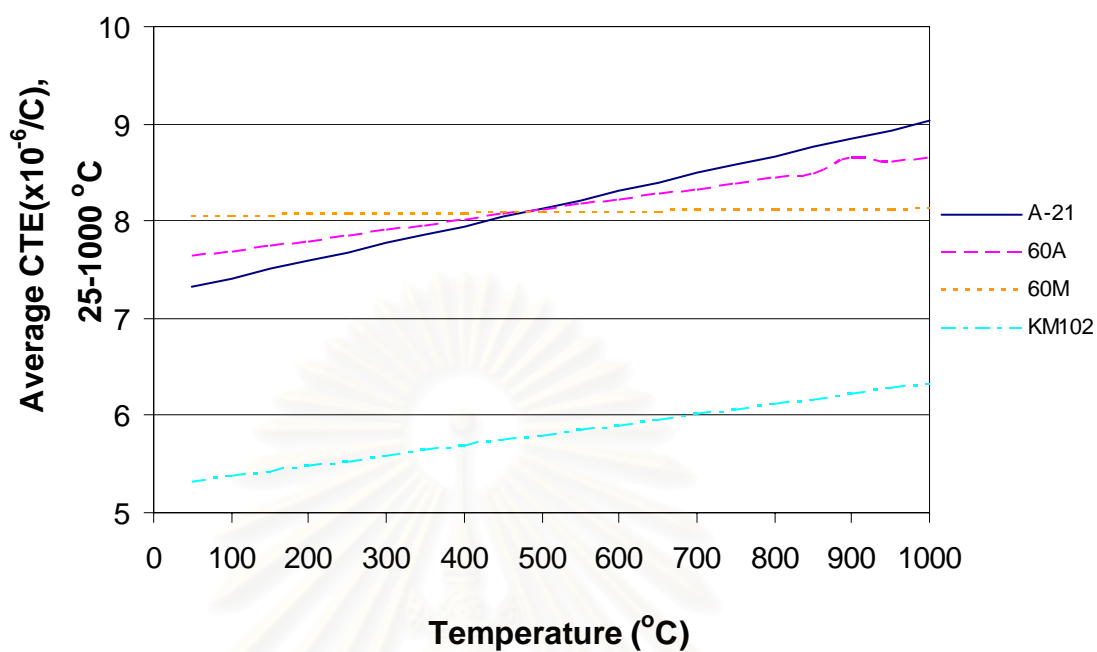
Fig. 4.9. Grain sizes of specimens sintered at 1650 and 1700 °C, 2h.

4.5.4 The coefficients of thermal expansion of the specimens

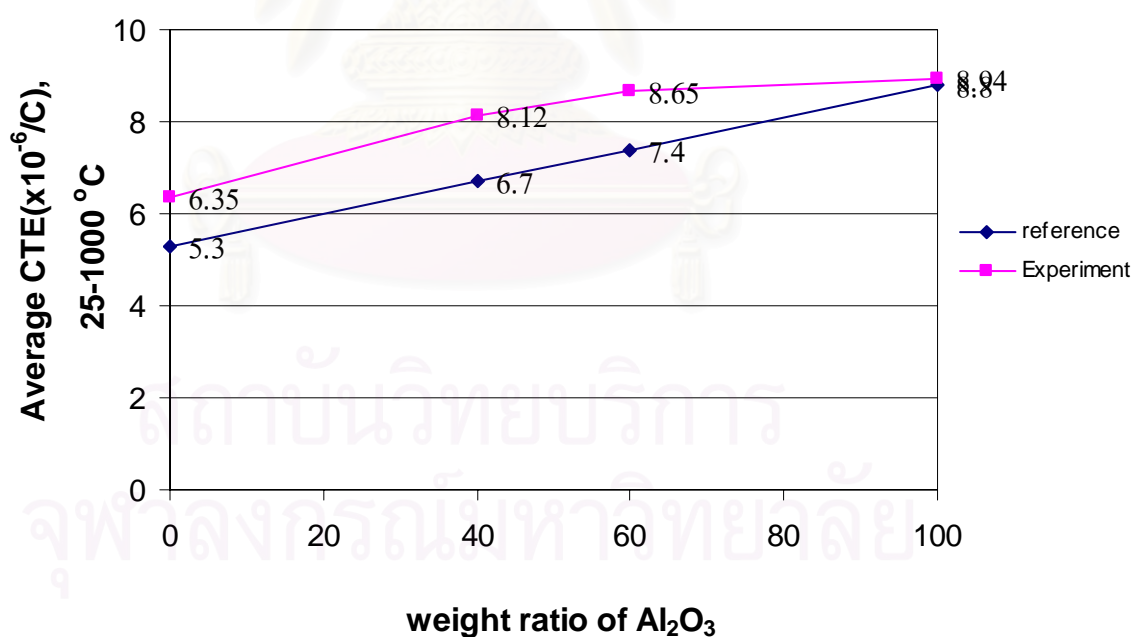
The coefficients of thermal expansion (CTE) of A-21(100A), KM102(100M) and composite of 60A40M and 40A60M specimens sintered at 1650 °C, 2 h, were measured by dilatometer at a temperature range of 25-1000 °C.

The values of average (CTE) of these specimens are about 8.94, 6.35, 8.65 and $8.12 \times 10^{-6} \text{ }^{\circ}\text{C}^{-1}$, respectively (as shown in the upper line of Fig. 4.10(b)). From Fig. 4.10(b), the CTE values measured by dilatometer are higher than the values from reference. For example, the CTE value of KM102(100M) from measurement is about $6.35 \times 10^{-6} \text{ }^{\circ}\text{C}^{-1}$. On the other hand, the CTE of pure mullite from reference is about $5.3 \times 10^{-6} \text{ }^{\circ}\text{C}^{-1}$ [3]. About 5 wt% of Al_2O_3 contaminated during milling process.

The 5 wt% contamination of Al_2O_3 will only increase the CTE of mullite from 5.3 to $5.5 \times 10^{-6} \text{ }^{\circ}\text{C}^{-1}$. Therefore, the value $6.35 \times 10^{-6} \text{ }^{\circ}\text{C}^{-1}$ can not explain by the contamination only. The difference can not be made clear, so far.



(a)



(b)

Fig. 4.10. The coefficients of thermal expansion (CTE) 25-1000 °C (a) at various temperatures (b) the comparison of CTE values between the experiment and reference

4.5.5 Young's modulus

Fig. 4.11 shows Young's modulus of specimens calculated by equation (3.10) and reference data. There is large difference between the measured values and the reference values. The reference values show two times higher than the measured values. This result may be caused by the error of the testing machine, because JIS recommends the blank test. However, we did not perform the blank test. Mr. Thanakorn who is now in Tokyo Institute of Technology informed that the correction by blank test in his experiment was about 200%.

From equation (3.10), the maximum Young's modulus for pure Al_2O_3 (100A) sintered at 1700 °C for 2h is 149 GPa. The minimum Young's modulus for 40A60M sintered at 1650 °C for 2h is 87 GPa. From Fig. 4.6(b). The minimum value should be caused by the low density.

In the comparison between die pressing and slip casting process, die press specimens show a little higher value than that of slip cast specimens. This is attributed from the trend of higher density in die-pressed specimens than slip cast specimens. All data are shown in the Appendix B (Table B-1).

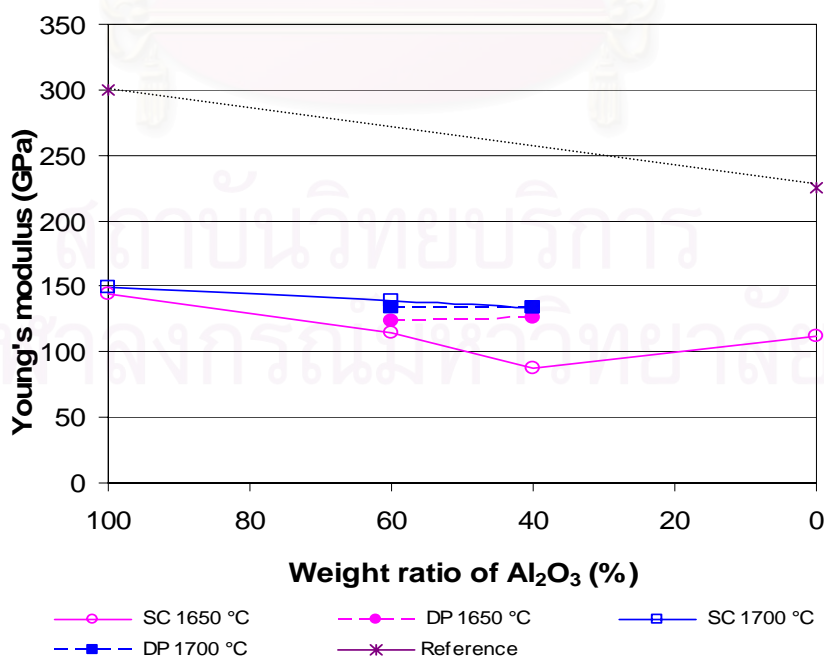


Fig. 4.11. Young's modulus of specimens formed by die pressing and slip casting, sintered at 1650°C and 1700°C for 2h.

4.5.6 Vickers hardness and fracture toughness

Fig. 4.10 shows the Vicker's hardness (Hv), calculated from equation (3.7) and reference values. Hv of Al_2O_3 is 20 GPa and that of mullite is 15 GPa in the literature. The maximum value for 60A40M, sintered at 1700°C for 2h is 17.9 GPa, from die pressing process. The Hv value of this composition depends on the microstructural features. High relative density, small grain size and equiaxial grain shape contribute to high Hv [7, 19]. In this sense, die press specimen shows a little higher Hv than slip cast specimen.

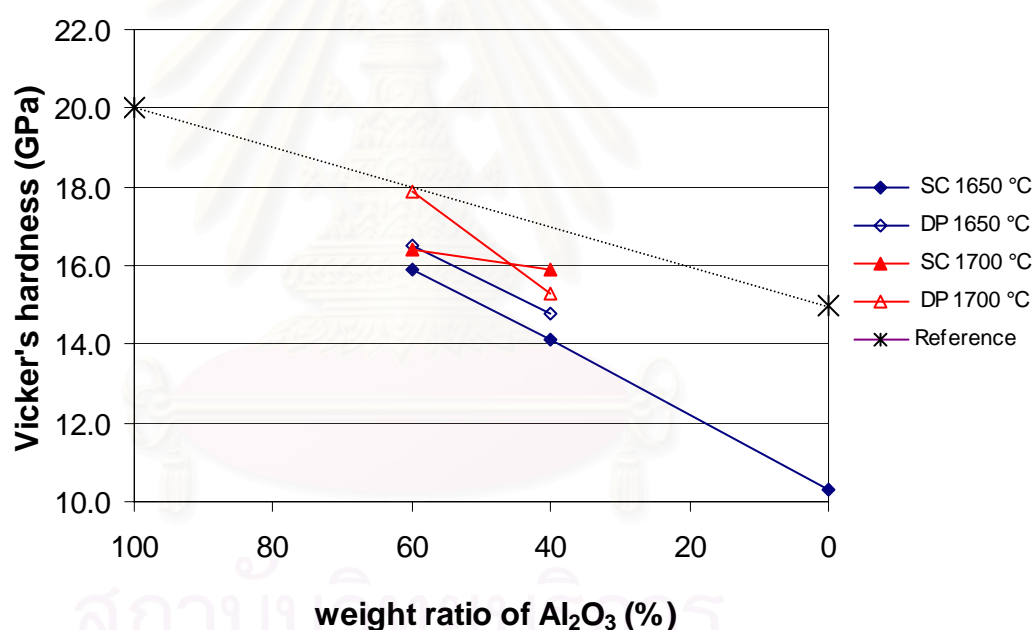


Fig. 4.12. Vicker's hardness of specimens formed by die pressing and slip casting processes.

Fig. 4.13 shows the fracture toughness of specimens calculated from equation (3.8). Fracture toughness increases with increasing the %weight ratio of Al_2O_3 .

The maximum value for 60A40M sintered at 1700°C for 2h is $4.4 \text{ MPa}\cdot\text{m}^{1/2}$, for slip cast specimen. This result can be supported by SEM micrographs as

shown in Fig. 4.14. Fig. 4.14 which reveal the difference of grain shape of the specimens from different processes. At the same composition and sintering temperature, the slip cast specimen shows much difference in grain sizes, elongated shape and porosity. On the other hand, the die press specimen shows an equiaxial grain shape and lower porosity. From these reasons, the increase of fracture toughness is related to the presence of the large difference in grain sizes, in the other word, inhomogeneous morphology might be the cause of large fracture toughness.

Generally, in a polycrystalline ceramic, grain boundary and pores can acts as barriers to propagation of crack. So that more work must be done to break the material. This explains why polycrystalline ceramics are tougher than glasses of the same composition [2].

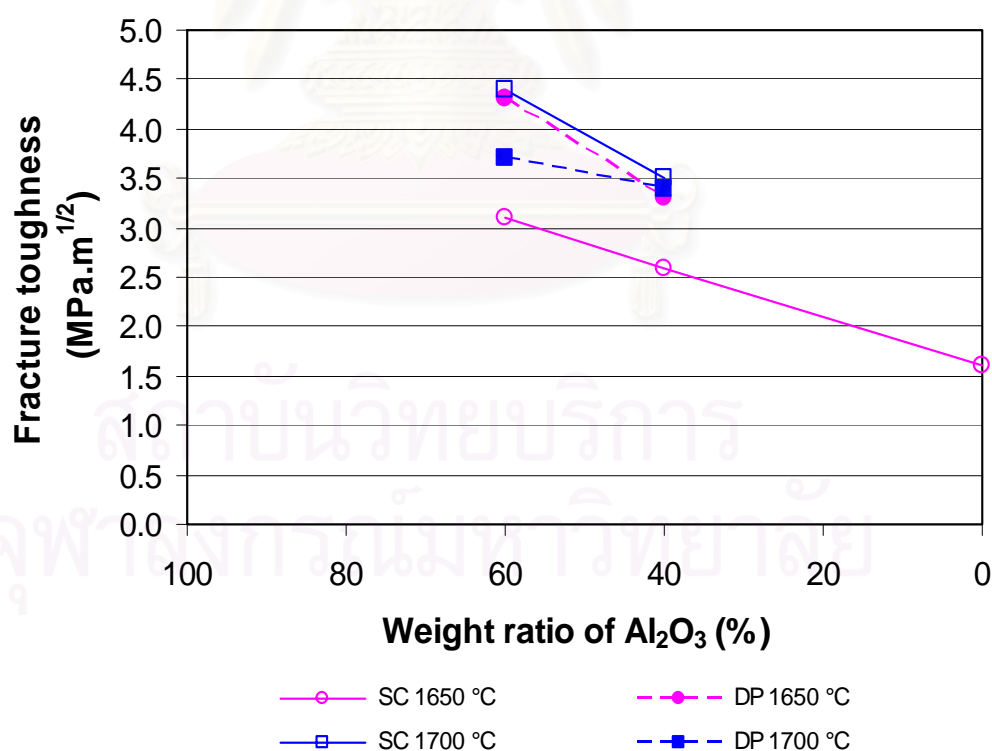
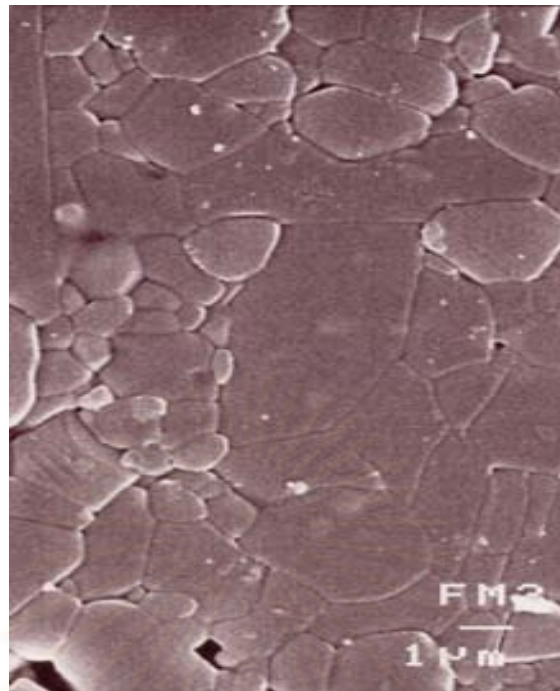
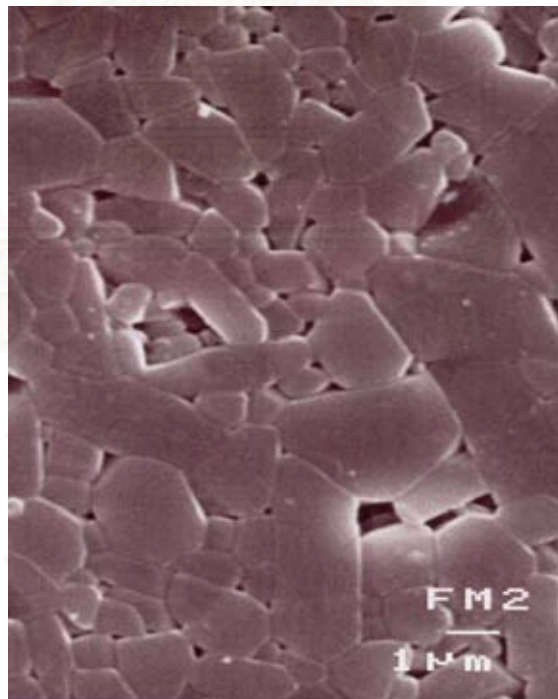


Fig. 4.13. Fracture toughness of specimens formed by die pressing and slip casting processes.



(a)



(b)

Fig. 4.14. SEM micrographs of 60A40M specimen sintered at 1700°C for 2h, (a) formed by die pressing and (b) formed by slip casting process.

4.5.7 Bending strength

Fig 4.15 and 4.16 show the bending strength (σ_{b4}) of specimens formed by slip casting and die pressing, respectively. All specimens were sintered at 1650°C and 1700°C for 2h. The σ_{b4} of specimens was calculated by equation (3.9). All data are shown in Appendix B (Table B-2) in details. For slip casting process, it is apparent that the σ_{b4} is related to the relative density (As shown in Fig. 4.6 (b)). The composite specimens at higher temperature show high σ_{b4} , exceeding 250 MPa. On the contrary, at lower temperature they show low σ_{b4} , less than 150 MPa. The maximum σ_{b4} of 40A60M, sintered at 1700°C for 2h is 282 MPa and the minimum σ_{b4} for 40A60M, sintered at 1650°C for 2h is 108 MPa. The low σ_{b4} is thought to come from big pores generated in the process of slip casting.

For die pressing process, is shown in Fig 4.16. At lower temperature composite with 40A60M shows maximum σ_{b4} , 245 MPa. But at higher temperature composite with 60A40M shows maximum σ_{b4} , 259 MPa. These results, are confirmed by SEM micrographs, as shown in Fig. 4.17.

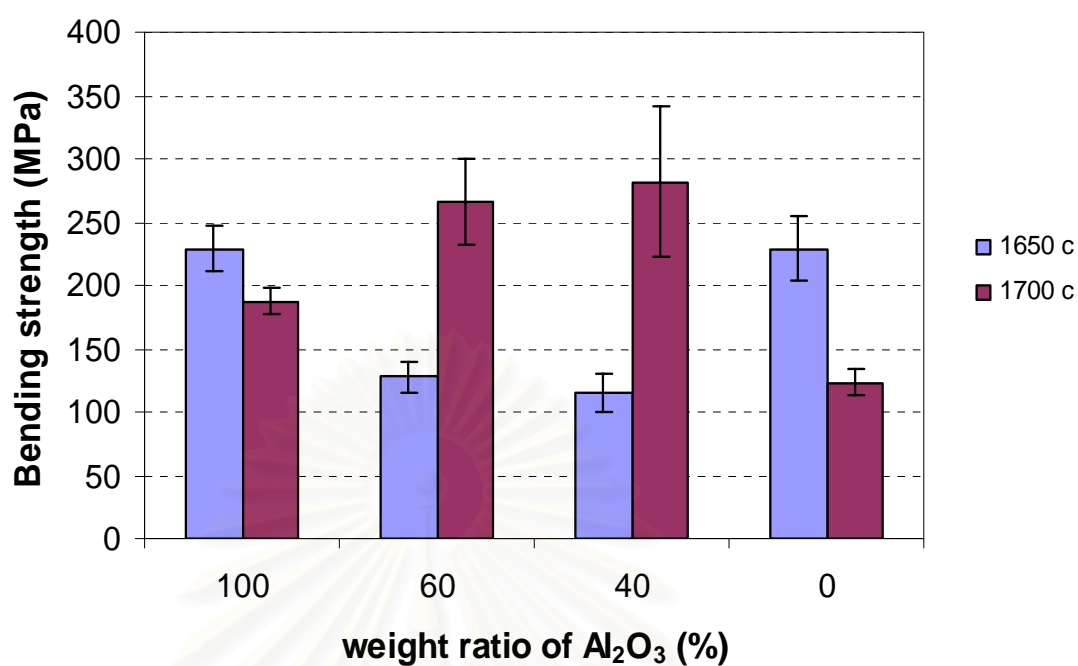


Fig. 4.15. Bending strength of specimens formed by slip casting, sintered at 1650°C and 1700°C for 2h.

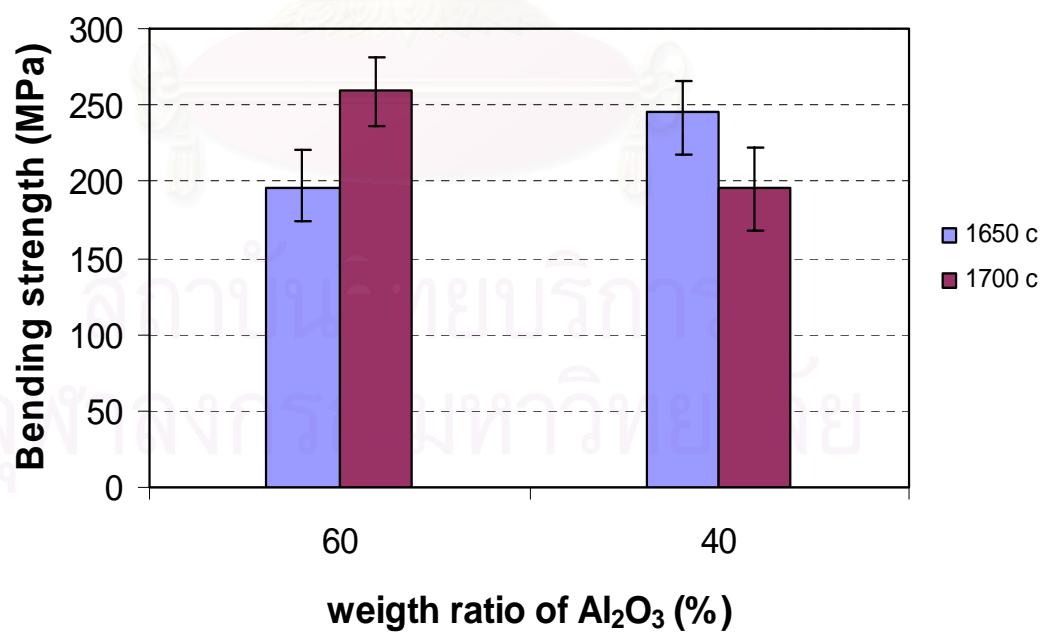


Fig. 4.16. Bending strength of specimens formed by die pressing, sintered at 1650°C and 1700°C for 2h.

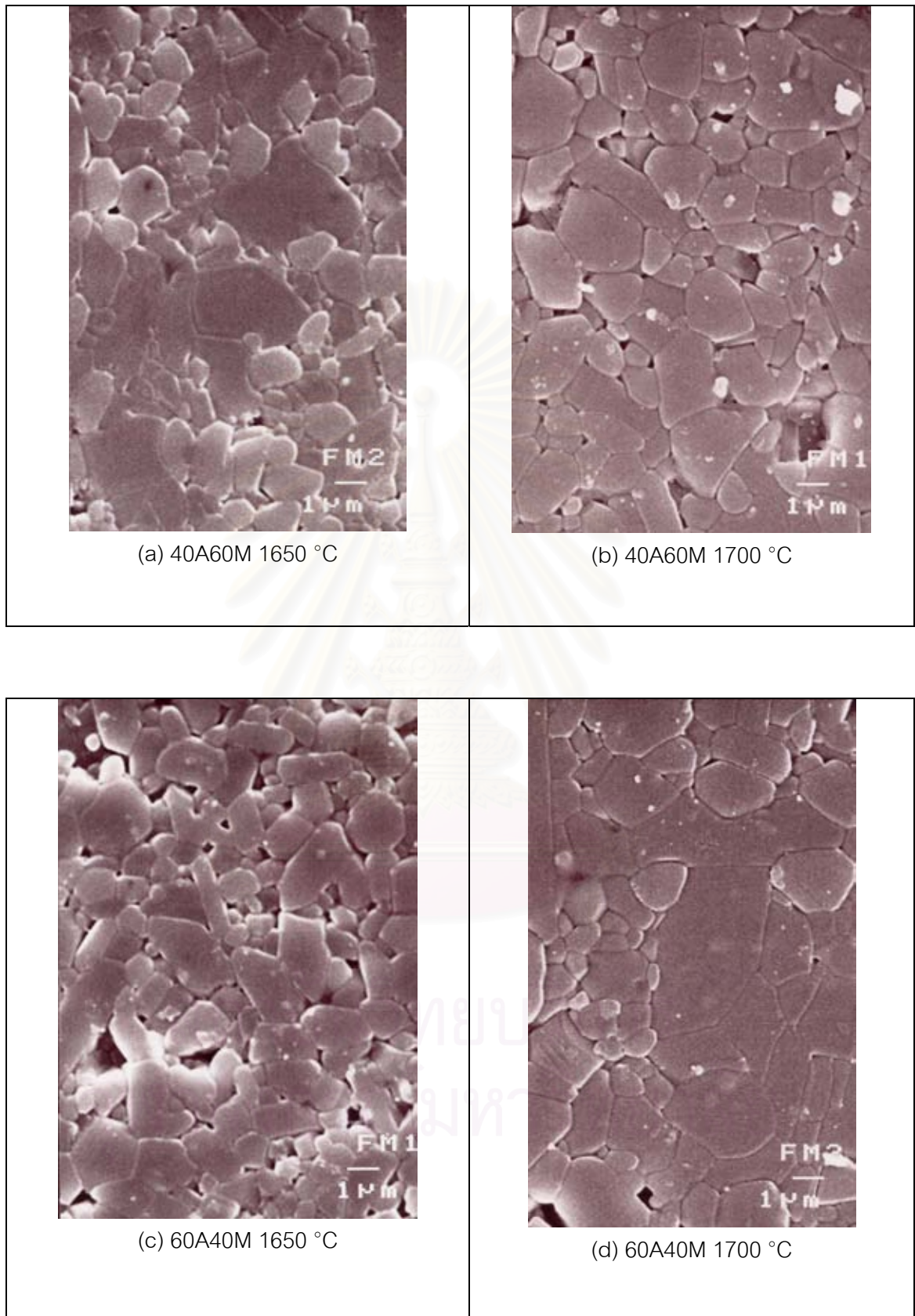


Fig. 4.17. SEM micrographs of composite specimens formed by die pressing process, sintered at 1650 °C and 1700 °C for 2 h.

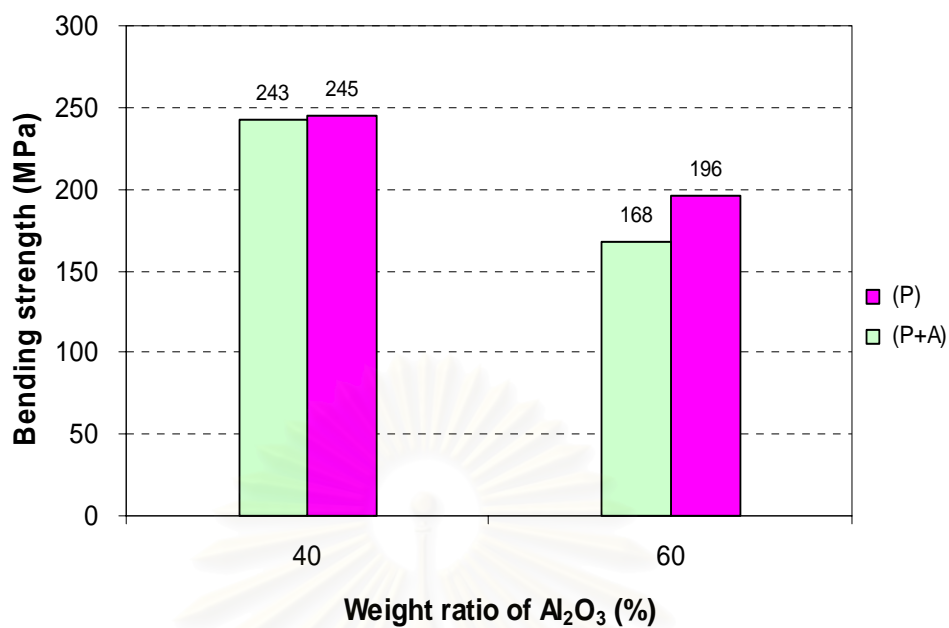


Fig. 4.18. Comparison of the bending strengths between only polished (P) and polished followed by annealing (P+A) of specimens formed by die pressing and sintered at 1650°C for 2h.

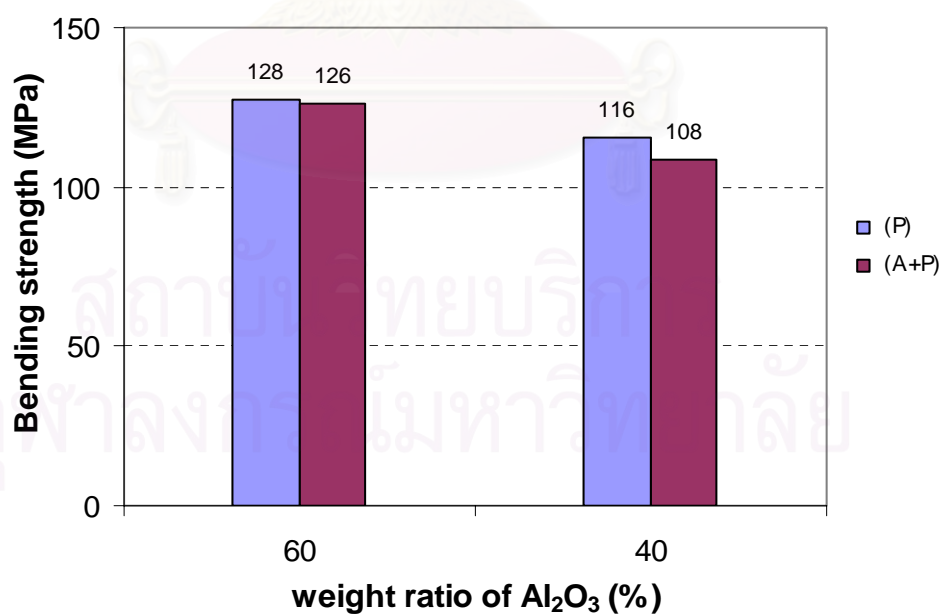


Fig. 4.19. Comparison of the bending strengths between only polished (P) and annealed followed by polishing (A+P) of specimens formed by slip casting and sintered at 1650°C for 2h.

Generally the bending strength of ceramics is affected by the furnace cracks. To know the effect of annealing for the composite specimens, they were annealed both before and after polishing. From Fig. 4.18 and 4.19, annealing before or after polishing does not affect the strength of all specimens.



สถาบันวิทยบริการ
จุฬาลงกรณ์มหาวิทยาลัย

CHAPTER 5

CONCLUSIONS

1. Sound figure of pre-stressed ceramics with hybrid structure of mullite and alumina could not be realized. Both die pressed pellet specimens and slip cast tube specimens cracked by the residual stress caused by the difference of thermal expansion. As a result, we concluded that this kind of hybrid structure was not a good solution to get high strength ceramics.
2. However, when outer layer was 40A60M and inner layer was 60A40M in the slip cast tube specimen e.g. it was the case compression stress in outer layer and the thermal expansion difference was not so much, specimens with no cracks were produced. From this result, when the thermal expansion difference was made smaller, there was some possibility that we can get sound figure with the compressed stress.
3. The composite with 40A60M showed (1) a homogeneous microstructure (without abnormal grain growth), (2) a rather higher K_{1c} of $4.4 \text{ MPa}\cdot\text{m}^{1/2}$ and (3) a good bending strength of 282 MPa.

CHAPTER 6

FUTURE WORK

In this experiment, we could not get a good hybrid ceramic, but found that Al_2O_3 /mullite composites showed some interesting characteristics such as homogeneous microstructure and possibility of good mechanical properties.

Then the following directions are recommended to survey more.

1. To find the better condition and fabrication technique to enhance the density at lower temperature.
2. To perform experiments on the composition of Al_2O_3 with small amount of mullite and mullite with small amount of Al_2O_3 .
3. In the experiment we did not add additives into the composites to improve fabrication process. Various types of additives should be able to raise the properties of composites.



สถาบันวิทยบริการ
จุฬาลงกรณ์มหาวิทยาลัย

REFERENCES

1. Adachi, T., Choa, Y. H., and Niihara, K. Crack Propagation Behavior of Nano- sized Dispersed Multilayered $\text{Al}_2\text{O}_3/3\text{Y-TZP}$ Hybrid Composites. J.Ceram. Soc. Jpn. 111(January 2003): 4-7.
2. Mencik, J. Strength and Fracture of Glass and Ceramics. Glass Science and Technology 12. Czechoslovakia: Elsevier Science Publishing Company, inc, 1992.
3. Kingery, W. D., Bowen, H. K., and Uhlmann, D. R. Introduction to Ceramics. Second edition. Singapore: John Wiley & Sons (SEA), 1991.
4. Fatigue crack Growth Behavior in Mullite/ Alumina Functionally Graded Ceramics. Available from: [Http://www.ceramicjournal.org](http://www.ceramicjournal.org).
5. Schneider, H., Okada K., and Pask, J.A. Mullite and Mullite Ceramics. England : John Wiley & Sons, 1994.
6. Yasuoka, M. et al. High-Strength and High-Fracture Toughness Ceramics in the $\text{Al}_2\text{O}_3/\text{LaAl}_{11}\text{O}_8$ Systems. J. Am. Ceram. Soc., 78 [July 1995]: 1853-1856.
7. William, E., Lee, D.P., and Rainforth, W. M. Ceramic Microstructures. First edition. London: Chapman & hall, 1994.
8. Awaji, H., Choi, S., and Yagi, E. Mechanism of toughening and strengthening in ceramic-based nanocomposites. Mechanics of Materials. 34(2002): 411- 422.
9. Jin, G., and Awaji, H. Residual Thermal stresses in multilayered Functionally Graded Material Plates. Material Science Research International. 9 (February 2003): 125-130.
10. Sivakumar, R. et al. Processing of mullite- molybdenum graded hollow cylinders by centrifugal molding technique. J. Eur. Ceram. Soc. 23 (2003): 765-772.
11. Aksel, C. The effect of mullite on the mechanical properties and thermal Shock behavior of alumina- mullite refractory materials. Ceramic International. 29(2003): 183-188.
12. Li, X. et al. Effect of powder Characteristics on Centrifugal Slip Casting of Alumina powders. J. Ceram. Soc. Jpn. 111(August 2003): 594-599.
13. Khan, A., Chan, M. H., and Harmer, M. P. Toughening of an Alumina-Mullite composite by Unbroken Bridging Elements. J. Am. Ceram. Soc. 83 (April 2000): 833-840.

14. Khan, A., Chan, M. H., and Harmer, M. P. Alumina agglomerate effects on Toughness- Curve Behavior of Alumina- Mullite composites. J. Am. Ceram. Soc. 83 (December 2000): 3089-3094.
15. Lec, S. Jin., and Kriven, W. M. Toughed oxide Composites Based on Porous Alumina- Platelet Interphases. J. Am. Ceram. Soc., 84 (April 2001): 767-774.
16. Awaji, H., and Ramasamar. Temperature and stress distributions in a Hollow cylinder of Functionally graded Materials: the case of Temperature- Independent Material Properties. J. Am. Ceram. Soc., 84 (May 2001): 1059-1065.
17. Chen, C., and Awaji, H. Transient and Residual Stress in a hollow cylinder of Functionally Graded Materials. Materials Science Forum. 423-425(2003): 665-670.
18. Biesheuvel, P. M., and Verweij, H. Calculation of the Composition Profile of a Functionally Graded Material Produced by Centrifugal Casting. J. Am. Ceram. Soc. 83 (April 2000): 743-749.
19. Wachtman, J. B. Mechanical Properties of Ceramics. The United States of America: John Wiley & Sons, 1996.
20. Varshneya, A. K. Fundamentals of inorganic glasses. New York: Brance & Company publishers, 1994.



Appendices

สถาบันวิทยบริการ
จุฬาลงกรณ์มหาวิทยาลัย



Appendix A

สถาบันวิทยบริการ
จุฬาลงกรณ์มหาวิทยาลัย

Table A-1. Bulk density, relative density and water absorption of slip cast specimens,
sintered at 1650 C for 2 h.

A-21 1650 C

| sample No. | Wd. | Wsat. | Wsus. | %Wa.ab. | Bulk.den | RD | %RD | True por. |
|------------|------|-------|-------|---------|----------|------|-------|-----------|
| 1 | 1.89 | 1.89 | 1.39 | 0.03 | 3.80 | 0.96 | 96.2 | 3.84 |
| 2 | 1.89 | 1.89 | 1.39 | 0.05 | 3.79 | 0.96 | 96.1 | 3.94 |
| 3 | 1.89 | 1.89 | 1.39 | 0.04 | 3.80 | 0.96 | 96.1 | 3.86 |
| 4 | 1.88 | 1.88 | 1.39 | 0.04 | 3.80 | 0.96 | 96.2 | 3.79 |
| 5 | 1.88 | 1.88 | 1.39 | 0.04 | 3.80 | 0.96 | 96.3 | 3.73 |
| 6 | 1.89 | 1.89 | 1.39 | 0.00 | 3.81 | 0.97 | 96.5 | 3.48 |
| 7 | 1.89 | 1.89 | 1.39 | 0.07 | 3.80 | 0.96 | 96.1 | 3.86 |
| AVE | | | | 0.04 | 3.80 | 0.96 | 96.21 | 3.79 |

60A/40M 1650 C

| | | | | | | | | |
|-----|------|------|------|------|------|------|-------|------|
| 1 | 1.60 | 1.60 | 1.14 | 0.05 | 3.43 | 0.94 | 94.0 | 5.95 |
| 2 | 1.60 | 1.60 | 1.14 | 0.07 | 3.45 | 0.95 | 94.6 | 5.41 |
| 3 | 1.58 | 1.59 | 1.13 | 0.08 | 3.45 | 0.95 | 94.5 | 5.47 |
| 4 | 1.61 | 1.61 | 1.14 | 0.02 | 3.45 | 0.95 | 94.6 | 5.43 |
| 5 | 1.62 | 1.62 | 1.15 | 0.06 | 3.46 | 0.95 | 94.9 | 5.11 |
| AVE | | | | 0.06 | 3.45 | 0.95 | 94.53 | 5.47 |

60M/40A 1650 C

| | | | | | | | | |
|-----|------|------|------|------|------|------|------|------|
| 1 | 1.52 | 1.52 | 1.06 | 0.16 | 3.28 | 0.94 | 93.6 | 6.36 |
| 2 | 1.53 | 1.53 | 1.07 | 0.10 | 3.34 | 0.95 | 95.3 | 4.65 |
| 3 | 1.49 | 1.50 | 1.04 | 0.10 | 3.23 | 0.92 | 92.2 | 7.79 |
| 4 | 1.51 | 1.51 | 1.07 | 0.07 | 3.42 | 0.98 | 97.8 | 2.16 |
| 5 | 1.50 | 1.50 | 1.04 | 0.11 | 3.27 | 0.94 | 93.6 | 6.43 |
| 6 | 1.50 | 1.52 | 1.08 | 0.12 | 3.43 | 0.98 | 98.0 | 2.05 |
| AVE | | | | 0.11 | 3.33 | 0.95 | 95.1 | 4.91 |

KM102 1650 C

| | | | | | | | | |
|-----|------|------|------|------|------|------|-------|------|
| 1 | 1.51 | 1.51 | 1.03 | 0.02 | 3.12 | 0.97 | 97.1 | 2.88 |
| 2 | 1.51 | 1.51 | 1.02 | 0.07 | 3.11 | 0.97 | 96.9 | 3.14 |
| 3 | 1.54 | 1.54 | 1.05 | 0.03 | 3.12 | 0.97 | 97.0 | 2.95 |
| 4 | 1.52 | 1.52 | 1.03 | 0.07 | 3.08 | 0.96 | 96.1 | 3.94 |
| 5 | 1.53 | 1.53 | 1.04 | 0.08 | 3.11 | 0.97 | 96.9 | 3.13 |
| AVE | | | | 0.05 | 3.11 | 0.97 | 96.79 | 3.21 |

Table A-1 (cont.). Bulk density, relative density and water absorption of slip cast specimens, sintered at 1700 C for 2 h.

A-21 1700 C

| sample No. | Wd. | Wsat. | Wsus. | %Wa.ab. | Bulk.den | RD | %RD | True por. |
|------------|------|-------|-------|---------|----------|------|-------|-----------|
| 1 | 1.95 | 1.95 | 1.44 | 0.03 | 3.84 | 0.97 | 97.2 | 2.77 |
| 2 | 1.98 | 1.98 | 1.46 | 0.04 | 3.84 | 0.97 | 97.2 | 2.77 |
| 3 | 1.98 | 1.98 | 1.47 | 0.04 | 3.83 | 0.97 | 97.0 | 2.99 |
| 4 | 1.97 | 1.97 | 1.46 | 0.06 | 3.83 | 0.97 | 97.0 | 3.02 |
| 5 | 1.97 | 1.97 | 1.46 | 0.05 | 3.83 | 0.97 | 97.1 | 2.91 |
| AVE | | | | 0.04 | 3.84 | 0.97 | 97.11 | 2.89 |

60A/40M 1700 C

| | | | | | | | | |
|-----|------|------|------|------|------|------|------|------|
| 1 | 1.70 | 1.71 | 1.23 | 0.05 | 3.56 | 0.90 | 90.2 | 9.83 |
| 2 | 1.70 | 1.70 | 1.23 | 0.05 | 3.56 | 0.90 | 90.2 | 9.81 |
| 3 | 1.66 | 1.66 | 1.19 | 0.02 | 3.56 | 0.90 | 90.2 | 9.81 |
| 4 | 1.68 | 1.68 | 1.21 | 0.04 | 3.57 | 0.90 | 90.3 | 9.67 |
| 5 | 1.65 | 1.65 | 1.19 | 0.03 | 3.56 | 0.90 | 90.2 | 9.82 |
| 6 | 1.65 | 1.66 | 1.19 | 0.03 | 3.56 | 0.90 | 90.3 | 9.75 |
| 7 | 1.65 | 1.65 | 1.19 | 0.01 | 3.57 | 0.90 | 90.3 | 9.72 |
| AVE | | | | 0.03 | 3.56 | 0.90 | 90.2 | 9.77 |

60M/40A 1700 C

| | | | | | | | | |
|-----|------|------|------|------|------|------|-------|------|
| 1 | 1.76 | 1.76 | 1.25 | 0.06 | 3.44 | 0.98 | 98.3 | 1.70 |
| 2 | 1.70 | 1.70 | 1.20 | 0.02 | 3.44 | 0.98 | 98.2 | 1.82 |
| 3 | 1.72 | 1.72 | 1.22 | 0.04 | 3.43 | 0.98 | 98.1 | 1.93 |
| AVE | | | | 0.04 | 3.44 | 0.98 | 98.18 | 1.82 |

KM102 1700 C

| | | | | | | | | |
|-----|------|------|------|------|------|------|-------|------|
| 1 | 1.46 | 1.46 | 0.99 | 0.03 | 3.09 | 0.96 | 96.2 | 3.77 |
| 2 | 1.48 | 1.48 | 1.00 | 0.06 | 3.09 | 0.96 | 96.4 | 3.63 |
| 3 | 1.44 | 1.44 | 0.98 | 0.06 | 3.07 | 0.96 | 95.7 | 4.35 |
| 4 | 1.50 | 1.50 | 1.01 | 0.01 | 3.09 | 0.96 | 96.4 | 3.61 |
| AVE | | | | 0.04 | 3.09 | 0.96 | 96.16 | 3.84 |



Appendix B

สถาบันวิทยบริการ
จุฬาลงกรณ์มหาวิทยาลัย

Table B-1. Relative density of specimens formed by die-pressing and slip casting processes sintered at 1650 C and 1700 C for 2 h.

| Process | Temperature | Samples | Bulk Density | %RD |
|--------------|-------------|---------|--------------|------|
| Slip casting | 1650 °C | 100A | 3.80 | 96.2 |
| | | 60A | 3.45 | 94.5 |
| | | 60M | 3.34 | 95.1 |
| | | 100M | 3.11 | 96.8 |
| | 1700 °C | 100A | 3.84 | 97.1 |
| | | 60A | 3.56 | 97.1 |
| | | '60M | 3.44 | 98.2 |
| | | 100M | 3.09 | 96.2 |

| Process | Temperature | Samples | Bulk Density | %RD |
|-----------|-------------|---------|--------------|------|
| Die press | 1650 °C | 60A | 3.47 | 95.1 |
| | | 60M | 3.38 | 96.4 |
| | 1700 °C | 60A | 3.46 | 94.2 |
| | | 60M | 3.35 | 95.7 |

สถาบันวิทยบริการ
จุฬาลงกรณ์มหาวิทยาลัย

Table B-2. Bending strength of specimens formed by die-pressing and slip casting processes sintered at 1650 C and 1700 C for 2 h.

| Process | Temperature | Samples | Ben. Stg.(Mpa) | |
|--------------|-------------|---------|----------------|--|
| Slip casting | 1650 °C | 100A | 229 | |
| | | 60A | 128 | |
| | | 40A | 116 | |
| | | 100M | 229 | |
| | | | | |
| | 1700 °C | 100A | 188 | |
| | | 60A | 265 | |
| | | 40A | 282 | |
| 100M | | 123 | | |

| Process | Temperature | Samples | Ben. Stg.(Mpa) |
|-----------|-------------|---------|----------------|
| Die press | 1650 °C | 60A | 196 |
| | | 40A | 245 |
| | 1700 °C | 60A | 259 |
| | | 40A | 195 |

สถาบันวิทยบริการ
จุฬาลงกรณ์มหาวิทยาลัย

Table B-3 Vickers hardness of slip cast specimens, sintered at 1650 C and 1700 C for 2 h.

Slip casting 1650 c

A-21 Too much of pores, cannot measured.

| specimen | Diagonal X | Diagonal Y | Crack X | Crack Y | Micron | | | | | ave© | Hv (GPa) |
|----------|------------|------------|---------|---------|------------|------------|--------|---------|---------|--------|-----------|
| | | | | | Diagonal X | Diagonal Y | ave(a) | Crack X | Crack Y | | |
| KM102 1 | 3.29 | 3.23 | 16.55 | 14.64 | 133.20 | 130.77 | 131.98 | 670.04 | 592.71 | 631.38 | 10.44 |
| 2 | 3.35 | 3.27 | 15.33 | 13.04 | 135.63 | 132.39 | 134.01 | 620.65 | 527.94 | 574.29 | 10.13 |
| Ave | | | | | | | 133.00 | | 0.22 | 602.83 | 10.28 |
| 60M 1 | 7.25 | 7.41 | 23.88 | 24.23 | 128.70 | 131.54 | 130.12 | 423.91 | 430.12 | 427.01 | 10.74 |
| 2 | 6.10 | 6.23 | 20.78 | 20.43 | 108.28 | 110.59 | 109.44 | 368.88 | 362.66 | 365.77 | 15.18 |
| 3 | 6.07 | 6.21 | 24.27 | 21.38 | 107.75 | 110.24 | 108.99 | 430.83 | 379.53 | 405.18 | 15.31 |
| 4 | 6.05 | 6.94 | 23.71 | 18.49 | 107.40 | 123.20 | 115.30 | 420.89 | 328.22 | 374.56 | 13.68 |
| 5 | 6.07 | 6.17 | 26.92 | 24.13 | 107.75 | 109.53 | 108.64 | 477.87 | 428.34 | 453.11 | 15.41 |
| Ave | | | | | | | 114.50 | | 1.99 | 405.12 | 14.06 |
| 60A 1 | 6.05 | 6.23 | 20.88 | 19.93 | 107.40 | 110.59 | 108.99 | 370.65 | 353.79 | 362.22 | 15.31 |
| 2 | 6.00 | 6.09 | 22.79 | 18.99 | 106.51 | 108.11 | 107.31 | 404.56 | 337.10 | 370.83 | 15.79 |
| 3 | 5.94 | 5.93 | 17.99 | 23.28 | 105.44 | 105.27 | 105.36 | 319.35 | 413.25 | 366.30 | 16.38 |
| 4 | 6.00 | 5.98 | 16.93 | 18.39 | 106.51 | 106.15 | 106.33 | 300.53 | 326.45 | 313.49 | 16.08 |
| Ave | | | | | | | 107.00 | | 0.46 | 353.21 | 15.89 |

Slip casting 1700 c

A-21 Too much of pore, cannot measured.

KM102 Too much of pore, cannot measured.

| | | | | | | | | | | | |
|-------|------|------|-------|-------|--------|--------|--------|--------|--------|--------|-------|
| 60M 1 | 5.98 | 6.07 | 20.57 | 17.00 | 106.15 | 107.75 | 106.95 | 365.15 | 301.78 | 333.46 | 15.90 |
| 2 | 5.94 | 6.01 | 18.52 | 19.69 | 105.44 | 106.69 | 106.07 | 328.76 | 349.53 | 339.14 | 16.17 |
| 3 | 6.17 | 5.98 | 18.34 | 15.42 | 109.53 | 106.15 | 107.84 | 325.56 | 273.73 | 299.64 | 15.64 |
| 4 | 6.09 | 5.98 | 20.46 | 15.06 | 108.11 | 106.15 | 107.13 | 363.20 | 267.34 | 315.27 | 15.85 |
| 5 | 6.14 | 5.93 | 18.77 | 15.03 | 108.99 | 105.27 | 107.13 | 333.20 | 266.80 | 300.00 | 15.85 |
| Ave | | | | | | | 107.02 | | 0.19 | 317.50 | 15.88 |
| 60A 1 | 4.63 | 4.76 | 13.30 | 12.67 | 103.87 | 106.69 | 105.28 | 298.36 | 284.18 | 291.27 | 16.41 |
| 2 | 4.63 | 4.67 | 12.51 | 12.04 | 103.89 | 104.72 | 104.30 | 280.75 | 270.20 | 275.47 | 16.72 |
| 3 | 4.76 | 4.71 | 10.59 | 12.71 | 106.69 | 105.64 | 106.17 | 237.71 | 285.15 | 261.43 | 16.13 |
| 4 | 4.59 | 4.83 | 11.18 | 13.17 | 102.95 | 108.44 | 105.70 | 250.82 | 295.45 | 273.13 | 16.28 |
| Ave | | | | | | | 105.36 | | 0.25 | 275.33 | 16.38 |

Table B-4 Vickers hardness of die press specimens, sintered at 1650 C and 1700 C for 2 h.

Die Pressong 1650 c

| specimen | Diagonal X | Diagonal Y | Crack X | Crack Y | Micron | | | | | ave© | Hv (GPa) | |
|----------|------------|------------|---------|---------|------------|------------|--------|---------|---------|--------|--------------|-------|
| | | | | | Diagonal X | Diagonal Y | ave(a) | Crack X | Crack Y | | | |
| 60A | 1 | 5.86 | 6.05 | 15.73 | 15.45 | 104.02 | 107.40 | 105.71 | 279.23 | 274.26 | 276.75 | 16.27 |
| | 2 | 5.98 | 5.89 | 14.50 | 14.39 | 106.15 | 104.56 | 105.36 | 257.40 | 255.44 | 256.42 | 16.38 |
| | 3 | 5.96 | 5.79 | 15.38 | 17.04 | 105.80 | 102.78 | 104.29 | 273.02 | 302.49 | 287.75 | 16.72 |
| | 4 | 5.93 | 5.98 | 18.59 | 17.43 | 105.27 | 106.15 | 105.71 | 330.00 | 309.41 | 319.70 | 16.27 |
| | 5 | 5.80 | 5.91 | 14.53 | 15.45 | 102.96 | 104.91 | 103.93 | 257.93 | 274.26 | 266.09 | 16.84 |
| Ave | | | | | | | | 105.00 | | 0.26 | 281.34 | 16.50 |
| 60M | 1 | 6.23 | 6.28 | 20.28 | 15.56 | 110.59 | 111.48 | 111.04 | 360.00 | 276.21 | 318.11 | 14.75 |
| | 2 | 6.37 | 6.31 | 23.64 | 15.95 | 113.08 | 112.01 | 112.54 | 419.64 | 283.14 | 351.39 | 14.36 |
| | 3 | 6.17 | 6.21 | 15.88 | 17.99 | 109.53 | 110.24 | 109.88 | 281.89 | 319.35 | 300.62 | 15.06 |
| | 4 | 6.12 | 6.21 | 20.32 | 21.27 | 108.64 | 110.24 | 109.44 | 360.71 | 377.57 | 369.14 | 15.18 |
| | 5 | 6.16 | 6.31 | 20.96 | 18.34 | 109.35 | 112.01 | 110.68 | 372.07 | 325.56 | 348.82 | 14.85 |
| Ave | | | | | | | | 110.72 | | 0.32 | 337.62 | 14.84 |

Die Pressong 1700 c

| | | | | | | | | | | | | |
|-----|---|------|------|-------|-------|--------|--------|--------|--------|--------|--------|-------|
| 60A | 1 | 4.55 | 4.63 | 12.79 | 11.80 | 102.00 | 103.78 | 102.89 | 287.03 | 264.84 | 275.93 | 17.18 |
| | 2 | 4.61 | 4.56 | 16.39 | 13.39 | 103.46 | 102.23 | 102.85 | 367.74 | 300.43 | 334.08 | 17.19 |
| | 3 | 4.61 | 4.72 | 16.77 | 13.78 | 103.46 | 105.95 | 104.71 | 376.34 | 309.15 | 342.74 | 16.59 |
| | 4 | 4.67 | 4.67 | 14.35 | 12.38 | 104.81 | 104.72 | 104.76 | 321.92 | 277.67 | 299.80 | 16.57 |
| | 5 | 4.13 | 4.00 | 10.46 | 11.72 | 92.56 | 89.84 | 91.20 | 234.66 | 262.98 | 248.82 | 21.86 |
| Ave | | | | | | | | 101.28 | | 2.25 | 300.28 | 17.88 |
| 60M | 1 | 4.80 | 4.92 | 16.64 | 14.29 | 107.61 | 110.33 | 108.97 | 373.40 | 320.69 | 347.04 | 15.31 |
| | 2 | 4.83 | 4.88 | 18.02 | 15.79 | 108.47 | 109.39 | 108.93 | 404.29 | 354.35 | 379.32 | 15.33 |
| | 3 | 4.71 | 5.00 | 14.81 | 13.67 | 105.75 | 112.19 | 108.97 | 332.22 | 306.66 | 319.44 | 15.31 |
| | 4 | 4.91 | 4.90 | 12.92 | 13.79 | 110.06 | 109.97 | 110.01 | 289.81 | 309.36 | 299.58 | 15.03 |
| | 5 | 4.72 | 4.89 | 15.36 | 10.94 | 105.95 | 109.70 | 107.83 | 344.61 | 245.47 | 295.04 | 15.64 |
| Ave | | | | | | | | 108.94 | | 0.22 | 328.09 | 15.32 |

BIOGRAPHY

Miss Weenusarin Intiya was born in Nakornphanom on 3rd May 1977. After graduating with a Bachelor's Degree in Ceramic Engineering from Faculty of Engineering, Suranaree University in 1999, she worked at National Metal and Materials Technology Center (MTEC) for 2 years. She continued a further study in Master's Degree in the field of Ceramic Technology at Chulalongkorn University in 2002 and graduated in 2004.



สถาบันวิทยบริการ
จุฬาลงกรณ์มหาวิทยาลัย